CHEMSUSCHEM

DOI: 10.1002/cssc.200800087

Oriented Nanostructures for Energy Conversion and Storage

Jun Liu,*[a] Guozhong Cao,*[b] Zhenguo Yang,*[a] Donghai Wang,[a] Dan Dubois,[a] Xiaodong Zhou,[a] Gordon L. Graff,[a] Larry R. Pederson,[a] and Ji-Guang Zhang[a]

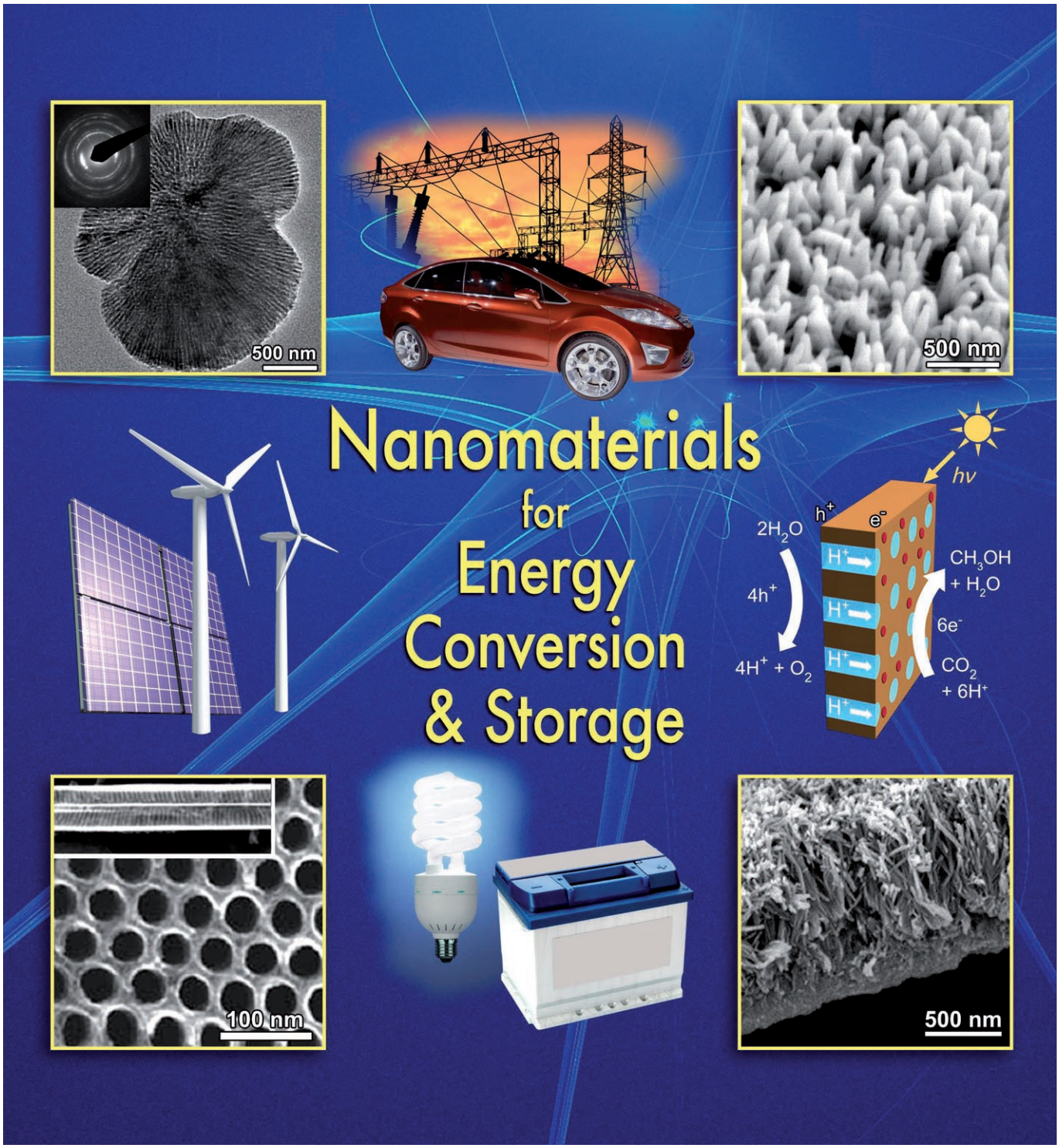

Recently, the role of nanostructured materials in addressing the challenges in energy and natural resources has attracted wide attention. In particular, oriented nanostructures demonstrate promising properties for energy harvesting, conversion, and storage. In this Review, we highlight the synthesis and application of oriented nanostructures in a few key areas of energy technologies, namely photovoltaics, batteries, supercapacitors, and thermoelectrics. Although the applications differ from field to field, a common fundamental challenge is to improve the generation and transport of electrons and ions. We highlight the role of high surface area to maximize the surface activity and discuss the importance of optimum dimension and architecture, controlled pore channels, and alignment of the nanocrystalline phase to optimize the transport of electrons and ions. Finally, we discuss the challenges in attaining integrated architectures to achieve the desired performance. Brief background information is provided for the relevant technologies, but the emphasis is focused mainly on the nanoscale effects of mostly inorganic-based materials and devices.

1. Introduction

The tremendous challenges in energy and natural resources are now widely recognized. According to recent studies,[1,2] the annual worldwide energy consumption is currently estimated to be 4.1×10^{20} joules, or 13 trillion watts (13 terawatts (TW)). Our energy is supplied from oil (35%), coal (23%), and natural gas (21%), which gives a total of around 80% from fossil fuels. Biomass makes up only 8% of the energy supply, nuclear energy accounts for 6.5%, and hydropower has a 2% share. The world population is predicted to reach 9 billion by 2050, and with aggressive conservation and new technology development the energy demand is predicted to double to 30 TW by 2050 and triple to 46 TW by the end of the century. At the same time, the oil production that is now the dominant energy supply is predicted to peak over the next 10 to 30 years. Coal accounts for about 50% of the electricity generated in the United States,[3] and it is believed that there is an abundant coal reserve to maintain the current consumption level for more than 100 years, but the certainty of the coal reserve has been disputed in some recent studies.[4] Moreover, new technologies need to be developed to capture the large amount of CO_2 produced by using coal which is currently already at 1.5 billion tons/year by the power plants in the United States alone.[3]

The impact of human activities on the environment is also a great concern. Within 200 years of industrialization, the level of CO_2 in the atmosphere has already increased from 280 ppm to 380 ppm. Industrial activities, mainly power generation from coal, have increased the total mercury flux from 1600 tons/year in the pre-industrial era to 5000 tons/year, of which 3000 tons is deposited in land and 2000 tons is deposited in marine.[5] The change in the climate and the aggressive measures to harness existing and alternative energy such as hydropower in developing countries also cause unprecedented problems in preserving the environment and natural resources. A study by the National Research Council estimated that currently 1.1 billion people are without access to safe drinking water and 2.2 billion people are without access to proper sanitation. In 2000 alone, 2.2 million deaths were attributed to water- and hygiene-related problems. By 2050, 4–7 billion people will face water scarcity.

There is no single solution to the daunting challenges we face concerning energy and environment. Significant progress has been made in the development of renewable energy technologies such as solar cells, fuel cells, and biofuels.[6–11] Although these alternative energy sources were marginalized in the past, it is expected that new technology could make them more practical and price-competitive with fossil fuels, enabling eventual transition away from fossil fuels as our primary energy sources. Almost all alternative energy technologies are limited by the properties of current materials. For example, poor charge-carrier mobilities and narrow absorption in current semiconductors limit the energy-conversion efficiency of photovoltaic cells.[12–25] Thermoelectric materials typically possess a figure of merit of less than 2.5.[26–28] Other electric power sources, such as batteries, supercapacitors, and fuel cells, do not have sufficient energy/power densities and/or efficiencies owing largely to poor charge- and mass-transport properties, and are too expensive as a result of materials and manufacturing costs.[29,30] Fundamental advances in the synthesis, processing, and control of multiscale structure and properties in advanced materials would usher in more efficient energy conversion and high-density energy/power-storage technologies.[31] Of great interests are nanotechnology and nanostructured materials, which are expected to have a great impact on semiconductors, energy, and the environmental, biomedical, and health sciences.[32] When a material is reduced to nanometer dimensions, its properties can be drastically different from its bulk properties. Recently, nanomaterials and novel designs based on nanomaterials have demonstrated very promising results for energy harvesting, conversion, and storage.[33,34]

Although the applications differ from field to field, one of the fundamental challenges is to develop oriented and controlled nanostructures to improve the generation and transport of electrons, ions, and other molecular species.[33,34] In this Review, first we briefly describe several major approaches to

[a] *Dr. J. Liu, Dr. Z. Yang, Dr. D. Wang, Dr. D. Dubois, Dr. X. Zhou, Dr. G. L. Graff, Dr. L. R. Pederson, Dr. J.-G. Zhang*
Pacific Northwest National Laboratory
Richland, WA 99352 (USA)
Fax: (+1) 509-375-3864
E-mail: jun.liu@pnl.gov
zgary.yang@pnl.gov

[b] *Prof. Dr. G. Z. Cao*
Department of Materials Science and Engineering
University of Washington, Seattle, WA 98195 (USA)
Fax: (+1) 206-543-3100
E-mail: gzcao@u.washington.edu

attain oriented nanostructured films that are applicable for energy applications. We also discuss how such controlled nanostructures can be used in photovoltaics, batteries, capacitors, thermoelectronics, and other unconventional methods of energy conversion. We highlight the role of high surface area to maximize the surface activity, and the importance of optimum dimension and architecture, controlled pore channels and alignment of the nanocrystalline phase to optimize electron and ion transport. Extensive research on the investigation of nanoparticles, nanopowders, and quantum dots is not included here. Brief background information is provided for the relevant technologies, but the emphasis will be on the nanoeffects (an extensive review of all topics and each specific application field is not attempted). Also, this Review focuses mainly on inorganic-based materials and devices, thus some other important research fields are not discussed here (e.g. organic photovoltaics, fuel cells, hydrogen generation and storage, and biofuels).

Jun Liu is a Laboratory Fellow at the Pacific Northwest National Laboratory (PNNL), where he currently leads the "Transformational Materials Science Initiative". He previously worked at Sandia National Laboratory and Lucent Bell Laboratory. His research interests include self-assembled nanomaterials and the synthesis and applications of nanostructured materials for energy, the environment, and medicine.

Guozhong Cao is Professor of Materials Science and Engineering and Adjunct Professor of Chemical and Mechanical Engineering at the University of Washington. He received his PhD from Eindhoven University of Technology. His current research is focused mainly on nanomaterials for energy-related applications including solar cells, lithium ion batteries, supercapacitors, and hydrogen storage.

Zhenguo Yang is a Chief Research Scientist at the PNNL, where he conducts fundamental and applied research into materials for energy storage and conversion. He is currently a technical leader in solid oxide fuel cell R&D and is also a principal investigator in the development of light-metal-based hydrides for hydrogen-storage applications and nanostructured materials for energy-storage applications.

2. Synthesis of Nanostructures and Oriented Nanostructured Films

2.1. Sol-Gel Processing

Sol-gel processing[35] is one of the most widely used methods, also often combined with hydrothermal growth, to prepare various nanostructured materials and films, such as those used in dye-sensitized solar cells.[36] Sol-gel processing is a solution method of making metal-oxide ceramic materials from alkoxide precursors or salts through controlled hydrolysis and condensation of the precursors. For example, TiO_2 nanoparticles and films can be obtained by treating titanium isopropoxide with water, followed by hydrothermal growth. Properties of the nanomaterial, such as the crystallinity, particle size, pore structure, surface area, and degree of agglomeration, depend on the reaction conditions, including the temperature, evaporation rate, drying conditions, and post-treatment. The rates of hydrolysis and condensation are largely affected by the type of precursors, the concentrations of acid and base, and the mixture of the solvents (water versus other solvents). The advantage of the sol-gel approach is the flexibility of the sol-gel chemistry and the wide range of microstructures that can be attained, from nanoparticles, nanostructured or nanoporous films, to nanostructured monoliths. To preserve the highly open and porous structure, supercritical drying is commonly applied for the removal of solvent. During the supercritical drying process, there exists no liquid–vapor interface and thus no capillary force; as a result, there is no capillary-force-driven collapse or shrinkage of highly open gel networks. Such sol-gel materials are referred to as aerogels,[37] which are highly porous with up to 99.9% porosity and specific surface areas over 1000 $m^2 g^{-1}$.

2.2. Direct Growth of Oriented Nanowire Arrays

The direct growth of large arrays of oriented nanowires has been extensively studied. For gas-phase syntheses, a vapor–liquid–solid (VLS) mechanism is the dominant method.[44] By this method, catalyst nanoparticles are first deposited on the substrate. The catalyst nanoparticle is melted and forms an alloy with one of the reacting elements in the vapor phase. The nanowires are nucleated from the catalyst nanoparticles. The size of the nanowires is determined by the size of the catalyst nanoparticles. The VLS method has been successfully used to prepare oriented carbon nanotubes,[45,46] oriented ZnO nanowires,[47,48] and many other materials. Low-temperature, solution-based synthesis is an alternative route to gas-phase synthesis that offers potential for large-scale and low-cost production and more systematic control of the nanostructures. Oriented ZnO nanowires and nanotubes are first prepared on bare glass substrates by controlling the nucleation, growth, and aging processes.[49,50] Lately, a seeded growth has been developed to grow oriented oxide and polymer nanowire arrays. In the seeded growth method, nanoparticles are first placed on the substrates.[38,51–55] The crystal growth is then carried out under mild conditions (low temperature and dilute concentra-

tion of the salt). Under these conditions, homogenous nucleation from the bulk solution is not favored and only heterogeneous nucleation on the supported nanoparticle seeds is allowed. Because the nanoparticles are the same as the materials to be grown, the low activation energy favors the epitaxial growth of the new one-dimensional materials (rods and wires) from the existing seeds. This approach avoids the difficulty in separating the nucleation and growth steps because the nucleation step is mostly eliminated. It is particularly suitable for multistep growth to produce complex nanostructures.[54,56–58] The size and density of the seeds to a large extent determine the size and population density of the nanowires or rods formed. This technique can be applied on a large scale to almost any surface. Figures 1a and 1b show the top and side view of large arrays of oriented conductive polymer nanowires grown directly from solution without using any templates.[38,39] As compared to oxides, polymer nanowires are very unusual because of their soft structure and have attracted wide attention recently.[59]

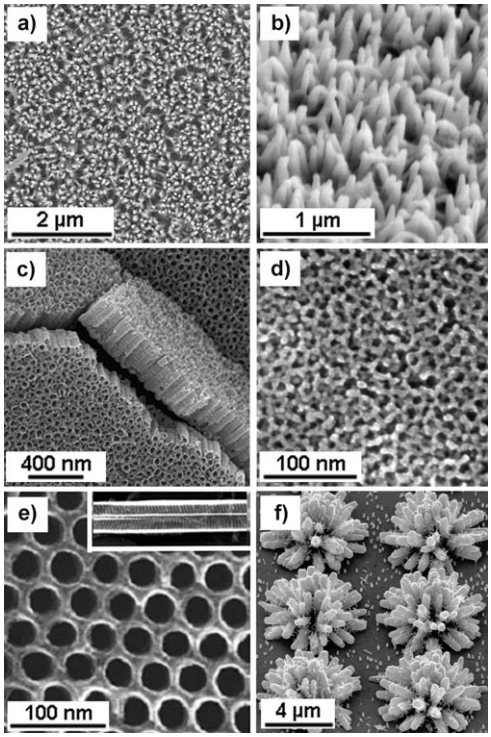

Figure 1. Electron microscopy images of selected examples of novel oriented nanostructures. a, b) Oriented conductive nanowires (polyaniline) prepared without using templates.[38,39] c) TiO_2 nanotube arrays prepared by anodization of Ti metal foils.[40] d) Mesoporous anatase TiO_2 templated by P123.[41] e) Oriented nanoporous carbon channels and films obtained from self-assembly approaches.[42] f) Ordered arrays of hierarchical ZnO nanostructures obtained by combining micropatterning and solution growth.[43]

2.3. Template Synthesis

The template approach has been extensively investigated to prepare supported or free-standing nanowires and nanotubes. The most commonly used and commercially available templates are anodized alumina membrane[60] and radiation track-etched polymer membranes.[61] Other membranes also have been used as templates, such as nanochannel-array glass,[61] radiation track-etched mica,[62] mesoporous materials,[63–67] porous silicon obtained by electrochemical etching of silicon wafer,[68] zeolites,[69]and carbon nanotubes.[70,71] Among the commonly used templates, alumina membranes with uniform and parallel porous structure are prepared by anodic oxidation of aluminum sheet in solutions of sulfuric, oxalic, or phosphoric acids.[60,72] The pores can be arranged in a regular hexagonal array, and densities as high as 10^{11} pores cm^{-2} can be achieved.[73] Pore sizes can range from 10 nm to 100 μm.[74,75] Polycarbonate membranes are made by bombarding a nonporous polycarbonate sheet, typically 6–20 μm in thickness, with nuclear fission fragments to create damage tracks and then by chemically etching these tracks into the pores.[76] In these radiation track-etched membranes, the pores have a uniform size as small as 10 nm although they are randomly distributed. Pore densities can be as high as 10^9 pores cm^{-2}. The templated approach is suitable for preparing nanoarrays of materials that are difficult to produce by using other solution techniques. For example, Bi_2Te_3 is of special interest as a thermoelectric material and Bi_2Te_3 nanowire arrays are believed to offer a higher figure of merit for thermal–electrical energy conversion.[77,78] Both polycrystalline and single-crystal Bi_2Te_3 nanowire arrays have been grown by electrochemical deposition inside anodic alumina membranes.[79,80] Sander and co-workers[79] fabricated Bi_2Te_3 nanowire arrays with diameters as small as about 25 nm.

2.4. Anodization

Anodization of thin metal films is a new technique to prepare oriented nanotube arrays (Figure 1c).[40] To prepare anatase TiO_2 nanotube arrays, a Ti metal film made of densely packed nanoparticles is first deposited over the entire substrate. A second Ti layer is deposited on top of the first layer, covering half of the surface. Anodization in an appropriate electrolyte solution by completely immersing the single-layer portion and contacting the two-layer region in the electrolyte produces well-oriented TiO_2 nanotube arrays in the single-layer region. By optimizing the growth conditions using ethylene glycol and NH_4F as the solvent, long titania nanotubes (1000 μm) could be prepare in the form of self-sustaining films (thickness of 1 mm).[81–83] The applications of such novel materials for solar energy conversion, photocatalysis, sensing, and medical implants have been investigated.[84,85]

2.5. Self-Assembly

Self-assembly principles have been widely investigated to fabricate organized nanostructures. Figure 1d shows an example of a mesoporous TiO_2 prepared by using P123 surfactant as the template.[41] In this approach, the surfactants and polymers self-assemble into ordered micellar structures owing to phase separation. Controlled pore channels can be obtained by removing the sacrificing phase.[86–88] These materials are charac-

terized by their well-ordered structures, tunable pore size from 2 to 50 nm, and simple preparation methods. However, achieving large-scale alignment of the pore channels is a great challenge. External factors, such as electrical[89–91] and magnetic fields,[92,93] mechanical shearing,[93,94] geometric confinement,[95] and solvent evaporation,[96] have been investigated to facilitate the alignment. Dai and co-workers reported the synthesis of large arrays of vertically oriented, ordered nanoporous carbon channels by dispersing and polymerizing the carbon precursors in a surfactant matrix (Figure 1 e).[42] The vertical alignment is likely caused by the action of surface tension and evaporation during self-assembly.

2.6. Top-Down Approach

The combination of bottom-up and top-down approaches is attractive for generating hierarchical structures. Two-dimensional patterns of oriented nanocrystals can be created by modifying the spatial distribution of the interfacial energy on a substrate. For example, Aizenberg and co-workers[97–99] investigated the combination of self-assembled monolayers (SAMs) and soft lithography (microstamping or microcontact printing) to prepare spatially controlled micropatterns of calcite crystals on a surface with precisely controlled location, nucleation density, size, orientation, and morphology. The mineral nucleation of calcite crystals was favored on acid-terminated regions but suppressed in methyl-terminated regions, where the influx of nutrients was maintained below saturation. Liu and co-workers applied similar microcontact printing techniques to grow oriented ZnO nanorods on patterned substrates.[43] Extended microarrays of carboxyl-terminated alkylthiols were printed on electron-beam-evaporated silver films. When the patterned silver substrates were placed in aqueous zinc nitrate solutions, oriented ZnO nanorods formed on the bare silver surface but not on the surface covered by the carboxylic acid groups. Using this approach, they were able to obtain patterned lines, dots, and a variety of structures and control the density and the spacing to micrometer scales (Figure 1 f).

3. Photovoltaics

3.1. Inorganic Solar Cells

Solar energy is considered as a carbon-neutral energy source and, thus, the ultimate solution to the energy and environmental challenge. Solar energy is the primary source of energy for all living organisms on earth. In one hour, the sun deposits 120 000 TW of radiation on the earth, more energy than we consume in a whole year.

Crystalline Si semiconductor photovoltaic cells were invented more than 50 years ago[100] and currently make up 90% of the market. Silicon photovoltaic cells operate on the principle of p–n junctions formed by joining p-type and n-type semiconductors. The electrons and holes are generated at the interface of p–n junctions, separated by the electrical field across the p–n junction, and collected through external circuits. The operation voltage is determined by the energy level of the electrons and holes leaving the cells.

Two significant challenges limit the widespread use of photovoltaics, namely the conversion efficiency of the cell and the cost. The cell conversion efficiency is defined as the ratio of the operating power density to the incident solar power density, and is mainly limited by the loss of excess energy of the excited electrons (the energy difference between the photons and the semiconductor band gap) in the form of thermal energy (the Shockley–Queisser limit).[101] Novel designs and materials to overcome this thermodynamic limit, and a cost reduction of 15 to 25 times, are desired.

The current status of photovoltaic technologies has been discussed in some excellent reviews,[12–15,25] and a brief discussion is provided below. In principle, the Si semiconductors can reach 92% of the theoretical attainable conversion (29% for Si, and 32% for GaAS), with possible 20% conversion efficiency in commercial designs. However, because of the high demand of crystalline Si with competition from the microelectronics industry and the high materials cost (Si accounts for 50% of the total cost of the module), thin-film photovoltaics have attracted wide attention.[14,102] For example, amorphous thin-film Si is a good candidate because the defect level (dangling Si bonds) can be controlled by hydrogenation and the band gap can be reduced so that the light-absorption efficiency can be much higher than that of Si.[103–111] Amorphous Si can be deposited on any substrate by gas-phase deposition, and the process can be scaled up. However, amorphous Si tends not to be stable and can lose up to 50% efficiency within the first 100 hours. Bridging the gap between single-crystalline Si and amorphous Si is the nanocrystalline, polycrystalline, or multicrystalline Si film.[112–115] Polycrystalline Si has a great potential because of low capital cost, high throughput, and less stringent requirements on the quality of the Si feedstock. Cadmium telluride (CdTe) is another leading polycrystalline film candidate for photovoltaics.[116–120] It has an ideal band gap (1.5 eV) for single-junction solar cells, and lends itself to a wide range of low-cost manufacturing process. Recently, CdTe was proposed for large-scale land applications in the United States at a total cost of 400 billion dollars over the next 30 years.[121] CdS/$CuInSe_2$ (CIS),[122–124] Cu(In,Ga)Se_2 (CIGS),[125] and Cu(In,Ga)(Se,S)$_2$ (CIGSS)[126,127] have received much attention because they are direct semiconductors, can be either p-type or n-type, have band gaps that match the solar spectrum, and display high optical absorbance. They have excellent stability, can be produced on large scales for megawatt applications, and are compatible with flexible substrates. The performances of the major different types of photovoltaic materials are summarized in reference [25], and the demonstrated efficiency ranges from about 10% for amorphous Si, 16% for CdTe, 19% for CIGS, 20% for polycrystalline Si, and 25% for crystalline Si.

Although second-generation photovoltaics are advancing rapidly and have the potential to match or surpass the performance of single-crystalline Si with reduced costs, meeting the long-term goal of very low cost ($0.4/kWh) and very high efficiency (over 32%) requires major breakthroughs in materials science and cell design.

One-dimensional semiconductors, such as CdSe, CdTe, GaAs, $CuInS_2$, and $CuInSe_2$, have been investigated as the active components in photovoltaics.[128] Their nanoscale confinement provides an additional means to control the band gap, therefore improving the photon-absorption efficiency, as well as the charge transfer in the materials and across the interfaces. However, in general, the preparation of such materials is difficult and the overall device architecture and fabrication remains a great challenge. Peng et al. prepared aligned single-crystalline Si nanowire arrays for photovoltaic applications.[129] The p-type Si nanowire arrays were prepared by a galvanic displacement process in a solution of HF and silver nitrate. The p–n junction was formed by thermal $POCl_3$ diffusion to convert the Si nanowires into n-type semiconductors. Such Si nanowires had excellent antireflecting properties. A power conversion efficiency of 9.31% and a fill factor of 0.65 were obtained. A low current-collecting efficiency of the front electrodes was believed to limit the overall efficiency.

3.2 Photoelectrochemical Solar Cells

In the early 1990s, a new class of dye-sensitized solar cells (DSSCs) was reported and showed surprisingly high efficiencies of over 4% given that very inexpensive TiO_2 was used as the bulk of the photovoltaic cells.[36,130] The DSSCs are similar to a traditional electrochemical cell and comprise a nanoporous semiconducting electrode made of sintered TiO_2 nanoparticles and a dye molecule (metal bipyridyl complex). Upon photoexcitation, the dye molecules generate electrons and holes and inject the electrons into the TiO_2 semiconductors. The excited dye cations are reduced to the neutral ground state by a liquid electrolyte (iodide/triiodide redox-active couple dissolved in an organic solvent). The triiodide to iodide cycle is completed by drawing the electrons from the counter electrode. Because of the simplicity of the device and the low cost of TiO_2 (which is essentially the same material used in paints), DSSCs display a great potential for large-scale applications. DSSCs have displayed a confirmed power conversion efficiency of over 10% and minimum degradation after long-term operation (over 1000 h at 60–80 °C),[131,132] with 15% efficiency observed following optimization of the material design.[133]

The performance of DSSCs depends on several key components of the cells. First, the dye molecules have strong optical absorbance in the visible light range. The excited dye molecules transfer the electron from the metal to the π^* orbital of the carboxylated bipyridyl ligand attached to the metal-oxide surface (anatase TiO_2), and then release the electrons to the oxide within 100 fs. The high-surface-area nanocrystalline oxides function as the anode for current collection. Typically, the anatase TiO_2 oxide film is derived from a sol-gel process and has a surface area of about 100 $m^2 g^{-1}$, 50% porosity by volume, and a crystal size of 15 nm. The nanocrystalline structure is critical for two reasons: 1) the large surface area and small size of the crystals are required to anchor a large amount of dye molecules on the semiconductor surfaces; 2) the electrons need to be effectively transferred before they are stopped by bulk or surface defects and the grain boundaries. The diffusion of the electrons in the nanocrystalline materials may be limited by the slow diffusion through different grains and by the trap states on the grain boundaries.

However, DSSCs still face significant challenges. First, even though the cost of the electrodes is low, the cost of the dye molecules is high. New, inexpensive dye molecules that can efficiently absorb sunlight in the visible range are being studied.[135] Second, the long-term stability, reliability, and cell operation are still under investigation, with great potential offered by using solid electrolytes rather than liquid electrolytes.[136] Finally, the long-standing efficiency of about 10% needs to be significantly increased. Many approaches have been investigated to increase the efficiency by developing dyes with more efficient and broader spectral response, by increasing the open-circuit voltage through manipulating the band gaps of the semiconductors and the redox agents, and significantly by increasing the diffusion length of the electrons in the semiconductors. Yang and co-workers introduced a new concept by replacing the nanocrystalline films with oriented, long high-density ZnO nanowires prepared from solution seeded synthesis.[53,134,137] The high surface area is favorable for trapping the dye molecules, and the electron transport in oriented nanowires should be orders of magnitude faster than percolation in polycrystalline films. Still, this approach produced a full sun efficiency of 1.5%, which was believed to be limited by the total available surface areas of the arrays and limited thickness (Figure 2).[138] More recently, Yang and co-workers reported that the efficiency could be increased to 2.25% by applying a thin crystalline TiO_2 coating.[139] The increase was attributed to the passivation of the surface trap sites and the energy barrier to repel the electrons from the surfaces.

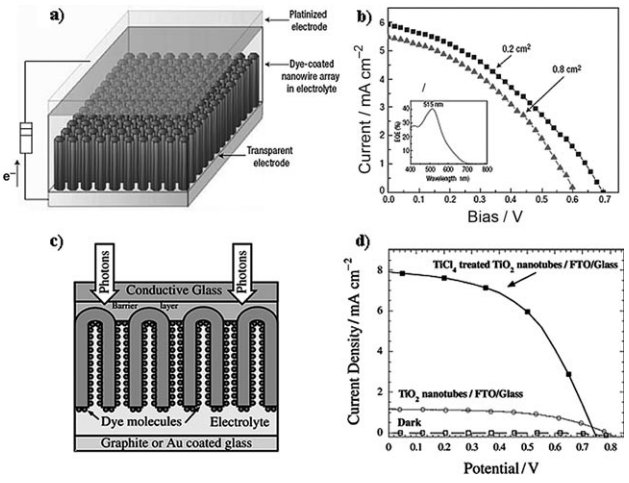

Figure 2. a, b) DSSCs based on ZnO nanowires: a) schematic diagram of the cell (transparent electrode/dye-coated nanowire array in electrolyte/platinized electrode), and b) current density as a function of bias. The inset shows the wavelength-dependent quantum efficiency (peak at 515 nm).[134] c, d) DSSCs based on anodized TiO_2 nanotubes:[40] c) architecture of TiO_2 nanotube based DSSCs, and d) photocurrent–voltage relationship.

Several groups have studied DSSCs using anodized, oriented TiO_2 nanotubes.[40] The oriented, transparent TiO_2 nanotubes

show a longer lifetime for the excited electrons and much slower recombination as a result of structural defects.[40,140] An efficiency of 2.9% was initially reported, maybe limited by the thickness of the film. Other oriented nanostructures, such as nanoarrays of TiO_2 nanowires and nanobelts from hydrothermal reactions, have also shown encouraging results for DSSCs.[141]

Even though the nanowire and nanotube arrays show fast electron transport, the limited density and thickness may prevent a much higher efficiency. To understand the challenges in this area, other approaches for high conversion efficiency on ZnO-based DSSCs through the controlled aggregation of ZnO nanocrystallites are compared. Zhang et al.[142–144] recently reported a noticeable progress in ZnO DSSCs through enhanced light scattering with controlled aggregation of ZnO nanocrystallites. In this approach, the primary ZnO nanocrystallites ensure the desired internal surface area for dye chemisorption, whereas the submicrometer spherical aggregates introduce light scattering so as to enhance photon absorption. The aggregates were intentionally prepared with a relatively wide size distribution to achieve better packing. It was also demonstrated that the surface smoothness of the submicrometer-sized aggregates has an appreciable impact on the conversion efficiency.

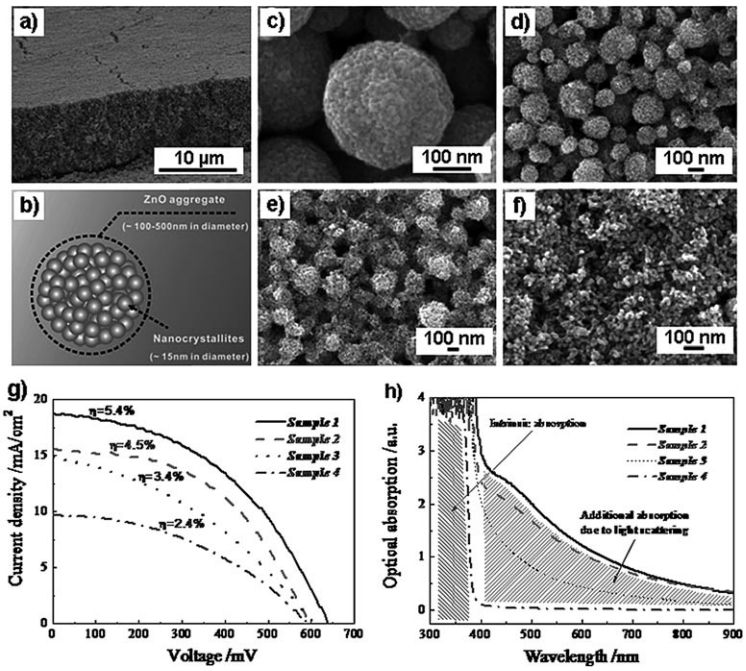

Figure 3. Controlled agglomeration of ZnO and resulting photovoltaic properties. a) Scanning electron microscopy (SEM) image of the cross-section showing the multilayered stacking of ZnO aggregates and the porous structure of the film. b) Schematic illustrating the microstructure of the ZnO aggregate and the closely packed aggregation of primary nanocrystallites. c–f) SEM images of samples 1, 2, 3, and 4 (see text for details) showing the deterioration in aggregation of nanocrystallites and their surface smoothness with increasing synthesis temperature (160, 170, 180, and 190 °C, respectively). g) Solar cell performance and optical absorption spectra of samples 1–4; conversion efficiencies (η) under AM 1.5 illumination decrease from 5.4% for sample 1 to 2.4% for sample 4. h) Spectra presenting the distinct optical absorption of all four samples in the UV/Vis region. The shaded part to the right corresponds to intrinsic absorption of ZnO; the shaded part to the right corresponds to additional absorption for samples caused by light scattering of ZnO aggregates.

Submicrometer-sized ZnO aggregates were synthesized by the hydrolysis of a zinc salt in a polyol medium at temperatures ranging from 160 °C to 190 °C, similar to the method reported by Jezequel et al.[145] The resulting colloidal dispersion was drop-cast onto a fluorine-doped tin oxide glass substrate to form a film of about 9 μm in thickness, and the film was then subsequently annealed at 350 °C for 1 h in air to remove residual solvents and any organics as well as to improve the contact and connection between the film and the substrate and between particles. Figure 3a shows the SEM images of ZnO aggregate film (denoted as sample 1), and Figure 3b shows a schematic illustrating the hierarchical structure. The uniform and well-packed films of submicrometer ZnO aggregates with almost perfect spherical shape and smooth surface can be seen in Figure 3c. Three other samples (samples 2, 3, and 4) were prepared at slightly higher temperatures, and their SEM images (Figure 3d–f) reveal deteriorating aggregation and increasing surface roughness of the aggregates. All of the ZnO samples exhibit the hexagonal Wurtzite structure with lattice constants $a = 0.32$ nm and $c = 0.52$ nm. Sample 2 was similar to sample 1, but it was made of ZnO aggregates with a slight disintegration on the aggregation of nanocrystallites, and moreover, an increased surface roughness (Figure 3d). Sample 3 was made of partial aggregates along with a dispersion of the primary ZnO nanocrystallites; most of the aggregates lost their spherical shape and hence significantly increased their surface roughness (Figure 3e). Sample 4 was a film made of dispersed primary ZnO nanocrystallites with no aggregates (Figure 3f). Nitrogen sorption analysis (Brunauer–Emmett–Teller (BET) surface area analysis) of the powder forms of all the samples revealed they all had similar internal surface areas of around 80 $m^2 g^{-1}$.

The ruthenium complex [*cis*-$RuL_2(NCS)_2$] (L = 2,2′-bipyridyl-4,4′-dicarboxylate) known as the N3 dye,[146,147] was used to sensitize the ZnO films. Adsorption of the dye was completed by immersing the films into a 0.5 mM solution of N3 dye in ethanol for about 20 min; this time was chosen to avoid the dissolution of surface Zn atoms and the formation of Zn^{2+}/dye complexes.[148] A comparison of current density and voltage behaviors revealed the difference in overall conversion efficiency for all four samples under AM 1.5 illumination. The highest conversion efficiency of 5.4% was obtained for sample 1, which comprised ideal spherical aggregates of ZnO nanocrystallites. The efficiency was reduced to 2.4% for sample 4, in which only dispersed ZnO nanocrystallites without aggregation were included. The spectra in Figure 3h present the distinct optical absorption of all four samples in the UV/Vis region. Slight humps are observed from the spectra of samples 1 and 2 around 400–500 nm. The shaded part on the right represents the additional absorption for sample 1, and partially for samples 2 and 3, caused by the light scattering of ZnO aggregates.

The shaded part on the left denotes the intrinsic absorption of ZnO. These results clearly suggest that the film thickness and the light scattering and absorption caused by the large aggregates contribute to the overall efficiency.

Several approaches have been pursued to overcome the Shockley–Queisser limit, including multijunction cells and multiexciton generation (MEG). In the multijunction cell, multiple absorbing layers of materials with different band gaps are arranged so that the band gap decreases layer by layer to maximize the photon absorption,[149,150] but the technology increases the cost of manufacturing and implementation. Another potential approach is to take advantage of the generation of multiple electron–holes (excitons) by one excitation event (MEG).[151–153] Multiexciton generation has been demonstrated for a range of zero-dimensional semiconductor quantum dots,[151,154–157] with photon-to-exciton conversion efficiencies of up to 700%.[158] However, it is not clear how the MEG effects can be used in a photovoltaic device and how the electrons can be collected. It remains to be seen if quantum dots can be integrated with some oriented architectures for the actual devices while retaining MEG properties, or if other materials of limited dimensionality (one-dimensional materials or nanowires) can also demonstrate multiexciton generation.

4. Electrical Energy Storage in Batteries

4.1. Introduction

Advanced electrical energy storage is a key technology to increase the efficiency in energy utilization, to promote the use of renewable energy, and to curb greenhouse gas emission.[159,160] Today, the primary storage technology is batteries that store electrical energy in chemical reactants capable of generating charges.[33,161,162] Energy storage in batteries is critical to the effective use of renewable energy generated from intermittent sources, such as solar and wind, and to the advance of electric vehicles, including plug-in-hybrid electric vehicles. However, the performance of current batteries falls short of requirements for their efficient use in these important application areas. While current electric vehicle batteries utilize nickel metal hydride (NiMH) technology, significant improvements are needed with regard to energy and power density, price, and lifetime. Although great progress has been made during the last 20 years in various battery systems, no current battery system can satisfy the targets set for electric vehicles, grid back-up, or other demanding applications. Among the most promising batteries are lithium ion batteries that offer high power and energy. However, their large-scale application is still limited by several barriers, including reliability, longevity, safety, and cost concerns.[163–167] Applications such as plug-in hybrid electric vehicles either require or prefer even higher energy/power than that offered by existing Li-ion batteries.

The performance of batteries strongly depends on the properties of their electrode and electrolyte materials. The emerging applications require revolutionary breakthroughs in the electrochemically active materials that enable a high voltage and multi-electrons per redox center for high energy density, improved charge transport and electrode kinetics, and satisfactory structural and interfacial stability, while being cost-effective. Nanomaterials have drawn great attention for their unusual electrochemical properties as compared to bulk materials with the same composition and crystalline structure. For Li ions as an example, nanomaterials as electrodes and electrolytes may provide advantages[33,34,168,299] including 1) better accommodation of the strain of lithium insertion/removal, improving the cycle life; 2) new reactions that are not possible in bulk materials; 3) a higher electrode–electrolyte contact area leading to a higher charge/discharge rate and thus a higher power; and 4) a short path distance for electron and Li^+ transport, permitting the battery to operate at higher power or to use materials with low electronic/ionic conductivity without adversely affecting power.

However, nanomaterials also introduce new challenges, including difficulties in manufacturing and handling of such materials, and very significantly, their stability and reliability under aggressive operation conditions. To fully exploit the advantages, the nanostructures of electrochemical active materials often need to be optimized with not only a small size but also desirable morphology, texture, and overall cell design.

4.2. Anodes in Li-Ion Batteries

Li_xSi exhibits great potential for this particular application (negative electrode) but needs a well-designed nanostructure to improve its structural and mechanical stability, and thus the stability of its electrochemical performance during charge/discharge processes. With a theoretical specific capacity of nearly 4200 mAh g^{-1} ($Li_{21}Si_5$), which is about ten times larger than the specific capacity of graphite (LiC_6, 372 mAh g^{-1}), Si has been proposed as one of the most promising candidates to replace the conventional graphite negative electrode. However, the high capacity of silicon is accompanied with huge changes in volume (up to 300%) upon alloying with lithium which can cause severe cracking and pulverization of the electrode and lead to significant capacity loss. Efforts have been made to mitigate this problem. One attractive approach is to create a nanocomposite microstructure that comprises an active lithium alloy phase uniformly dispersed in an inert host matrix, such as Si/C, Si/TiB_2, or Si/TiN composite materials.[169,170] Approaches including chemical vapor deposition, pyrolysis of Si-containing organic compounds, or mechanochemical methods have been used to fabricate the nanocomposites. During Li charging/discharging, the carbon phase acts as a buffer material (and a low-resistant electron path as well) to accommodate the volume change of silicon and mitigate the mechanical strain/stress, thereby improving the cycle life. Alternatively, multilayer concepts have also been tried to reduce the enormous mechanical stresses upon electrochemical cycling by introducing a series of 'buffer' layers between the active materials. Besides the small size, also the structure and morphology appeared to be important to the structural stability and electrochemical performance of the Si anode. Obrovac and Christensen[171] indicated that highly lithiated amorphous silicon rapidly crystallizes at 50 mV to form a new lithium–silicon phase, identified as

$Li_{15}Si_4$. In another study, Dahn and Hatchard[172] investigated the formation of crystalline silicon using an in situ X-ray probe and found that the electrochemically induced crystalline phase only forms on amorphous Si with a thickness of approximately 2 μm or above. These results raised the hope that amorphous Si might have the potential to avoid crystallization during the lithiation process and minimize capacity loss during repeated transformation between the crystalline and amorphous forms.

Despite the varied extent of improvement, the aforementioned efforts fell short of overcoming the pulverization issue associated with Si anodes. Recently, Yonezu et al.[173] (SANYO Electric Co., Ltd) reported that an amorphous Si (a-Si) film sputtered on a moderately roughened surface of copper foil could display virtually 100% reversibility over a capacity greater than 3000 mAh g^{-1} (see Figure 4a, b). The as-deposited amorphous

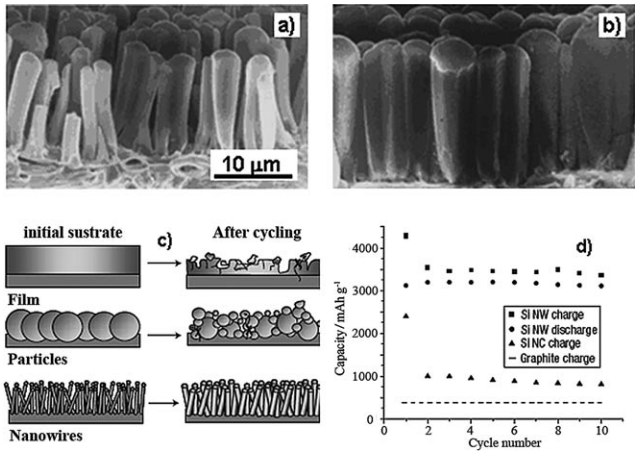

Figure 4. a, b) Cross-sectional SEM images of an amorphous silica (a-Si) thin-film electrode in the discharged (a) and charged state (b) with over 3000 mAh g^{-1} reversible capacity (part (b) is shown to the same scale as part (a)).[173] c) Comparison of conventional Si powders and Si nanowires during charge–discharge cycles.[174] d) Variation in capacity of Si nanowires over 10 cycles.[174]

Si film swelled in thickness and divided into microcolumns. The column structure demonstrated much improved structural and electrochemical stability, illustrating the importance of the morphology of electrode materials. The advantages of oriented Si nanostructures were further confirmed on oriented Si nanowires. Chan et al. used a VLS method to prepare oriented Si and Ge nanowires on a steel substrate using gold catalysts.[174,175] The prepared Si nanowires (diameter $<$ 100 nm) were capable of charging up to the theoretical capacity during the initial lithium insertion without pulverization (see Figure 4c, d). After transforming into amorphous Li_xSi, the one-dimensional nanosilicon electrode thereafter maintained a charge capacity of 75% of its theoretical capacity, with little fading after 10 cycles. Also, the shortened distance of lithium transport in the silicon nanostructure and low-resistance electrical connection led to an excellent rate capability ($>$ 2100 mAh g^{-1} at 1 C). The proof-of-concept study demonstrated that one-dimensional Si nanostructures could be promising anode materials for Li-ion batteries. Nonetheless, there is a need to develop cost-effective, practical approaches that can be used to produce high-performance silicon anodes.

As illustrated with the Si anodes, oriented nanostructuring can lead to improvements in structural and electrochemical performance, as well as in kinetics owing to shortened diffusion distances. For many materials including Si, however, the advantages are often accompanied by increased side reactions with the electrolyte as a result of the increased surface, raising concerns over safety and calendar life. In comparison, TiO_2, with a potential around 1.5 V (vs. Li^+/Li redox couple), is inherently safe in comparison to the graphite anode, which has an operating voltage close to that of Li electroplating and thus an issue of safety. However, the poor lithium-ion conductivity and electron conductivity of TiO_2 polymorphs limit their electrochemical activity of Li insertion. For example, as the most thermodynamically stable polymorph of TiO_2, rutile in its bulk crystalline form can only accommodate negligible Li ($<$ 0.1 Li ions per TiO_2 unit) at room temperature.[176,177] Recent studies indicated that diffusion of Li in rutile is highly anisotropic, which proceeds through rapid diffusion along *c* axis channels,[178,179] but it is very slow or difficult in the *ab* planes, preventing Li ions from reaching the thermodynamically favorable octahedral sites and separates Li in the *c* axis channels. Furthermore, the impulsive Li–Li interactions in the *c* axis channels together with the trapped Li-ion pairs in the *ab* planes may block the *c* axis channels and prevent further insertion. Interestingly, however, several groups,[180–183] recently reported that nanometer-sized TiO_2 (50 nm) can be an effective lithium ion insertion electrode. It appears that decreasing the TiO_2 particle size alters its reactivity towards Li, with no insertion observed for large particles as compared to the appearance of two solid solution domains and then the formation of electroactive rock-salt-type $LiTiO_2$. The reversible capacity of the nanorutile particles was up to 0.5 Li per oxide, which is comparable to that of anatase, another form of TiO_2. Similarly, Jiang et al.[183]reported recently that Li insertion can be up to Li/Ti = 1:1 in a rutile nano-electrode at the first discharge cycled at 0.05 A g^{-1}, and about 0.6–0.7 Li ions can be reversibly cycled. After 100 cycles, the discharge capacity of the ultrafine nanorutile electrodes remained at 132 and 118 mAh g^{-1} when cycled at 5 and 10 A g^{-1}, respectively. In addition, a similar size effect on materials electrochemical activity was also observed for nanosized anatase, for which a solid solution domain was observed prior to the classical biphasic transition.[184] These new findings provide justification to reinvestigate nanoscale structures of other electrode materials that display poor performance when used in their bulk form and open avenues to develop high-performance electrode materials.

Note that the nanosized rutiles with good Li-intercalation properties are mostly in the form of nanorods. Owing to the fact that Li diffusion is anisotropic in rutile, being particularly slow in the *ab* plane, the rutile nanorods along the [001] directions may be favorable for fast Li intercalation. The morphology effects were clearly demonstrated in studies by Meier and co-workers as shown in Figure 5a–f.[181] Recently, Wang et al.[185] described the synthesis of highly crystalline mesoporous rutile through a low-temperature solution approach. The nanostruc-

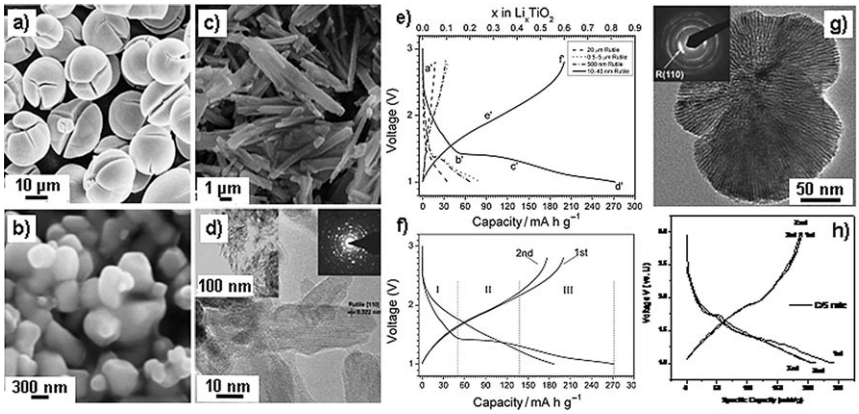

Figure 5. a–c) SEM images of different rutile particles: a) 20 μm particles; b) 500 nm particles; and c) rutile nanorods. d) High-resolution TEM images of rutile nanorods. e) Voltage profile of different rutile particles at *C*/20 rate. f) The first two cycles of intercalation/deintercalation. g) Mesoporous rutile made of oriented nanorods. h) The first three charge–discharge cycles of mesoporous rutile at *C*/5 rate.[185] (Parts (a)–(f) are reproduced from Ref. [181].)

tured rutile made of aligned rutile nanorod building blocks grown along the [001] direction was capable of accommodating more than 0.7 Li ions ($Li_{0.7}TiO_2$, 235 mAh g^{-1}) during the first charge at a rate of *C*/5 over 1–3 V (versus Li^+/Li) and thereafter exhibited a reversible capacity of 0.55 Li ions ($Li_{0.55}TiO_2$, 185 mAh g^{-1}). As shown in Figure 5 g, h, the mesoporous crystalline rutile exhibited excellent capacity retention with less than 10% capacity loss after 100 cycles. The study indicated that the rutile nanorods were transformed into cubic rock salt $LiTiO_2$ nanorods, but the mesostructures remained stable after the phase transformation and cycling.

Cao and co-workers[186–188] prepared and investigated acidic anodized TiO_2 nanotube arrays (Figure 6 a, d). Different morphologies of the nanotube arrays were obtained by optimizing the electrolyte solution. Subsequent thermal annealing converted the initially amorphous TiO_2 nanotube arrays into anatase TiO_2 at moderate temperatures of 300 °C and into rutile TiO_2 at higher temperatures (> 600 °C). Both amorphous and pure crystalline anatase TiO_2 exhibited poor Li^+-ion intercalation capacities, as well as rapid degradation during cycling. The best capacity with good cyclic stability was obtained with partially crystallized TiO_2 nanotube arrays that were annealed around 300 °C for 3 h, particularly for samples annealed in a nitrogen atmosphere. Annealing TiO_2 under nitrogen is known to result in N-doping and is likely the cause for the improved electrochemical properties of such grown TiO_2 nanotube arrays. Kim and Cho further compared the electrochemical performance of anatase nanotubes and nanorods which were synthesized by annealing mixed $H_2Ti_2O_5 \cdot H_2O$ and anatase TiO_2 nanotubes at 300 and 400 °C, respectively.[189] The tubelike nanostructure of anatase exhibited a capacity of 296 mAh g^{-1} as compared to 215 mAh g^{-1} for the rod form, and a much higher capacity retention.

Besides rutile and anatase, the importance of the size and morphologies was also demonstrated in spinel $Li_4Ti_5O_{12}$[190,191] and TiO_2-B.[192–195] For instance, Bruce and co-workers[193–195] reported a TiO_2-B nanowire anode that was capable of insertion up to $Li_{0.9}TiO_2$ (305 mAh g^{-1}) without noticeable structural degradation and change in the nanowire morphology. This capacity was delivered at a potential of around 1.6 V (vs Li^+(1 M)/Li) and the potential was relatively flat over most of the range. Cycling efficiency was excellent, as was the capacity retention. Interestingly, the rate capability was better than that for the same phase prepared as nanoparticles with dimensions similar to the diameter of the nanowires. Therefore, the nanowires and nanofibers have favorable properties for Li-ion intercalation.

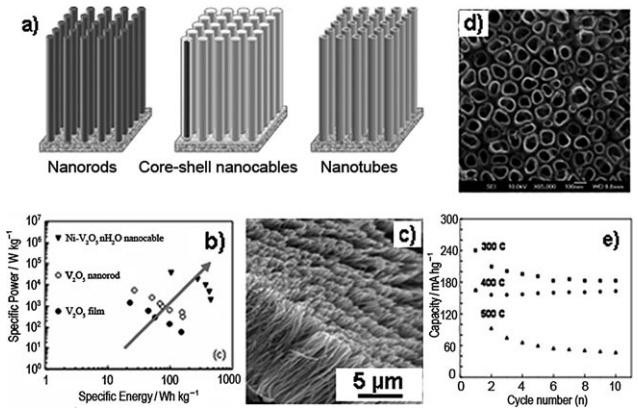

Figure 6. a) Schematic of nanorod, nanocable array, and nanotube electrodes for energy storage. b) Comparison of specific energy and specific power of V_2O_5 electrodes in the form of films, nanorods, and nanocable arrays. c) SEM images of oxide nanorod arrays. d) SEM image of TiO_2 nanotube arrays fabricated by acidic anodization and subsequently annealed in nitrogen at 300 °C for 3 h. e) Li-ion intercalation capacity as a function of charge–discharge cycles.

4.3. Cathodes in Li-Ion Batteries

The favorable electrochemical performance from one-dimensional nanostructures was also reported in other oxide systems for cathodes. For example, Cao and co-workers synthesized and characterized various one dimensional nanostructured electrodes of orthorhombic V_2O_5 and low-crystalline $V_2O_5 \cdot n H_2O$, including single-crystal V_2O_5 nanorod arrays,[196–198] $V_2O_5 \cdot n H_2O$, $InVO_4$, and TiO_2 nanotube arrays,[197,199,200] and Ni-$V_2O_5 \cdot n H_2O$ core–shell nanocable arrays.[201] The fabrication of such nanostructures was accomplished using template-based growth by sol electrophoretic deposition[202–208] and electrochemical deposition.[209–212] Furthermore, platelet and fibrillar nanostructured V_2O_5 films have been fabricated by solution-based methods.[186] These platelet and fibrillar films consist of randomly oriented nanoscale V_2O_5 particles or nanoscale fibers protruding from the substrate surface. These nanostructured

films exhibit larger surface areas and shorter diffusion paths for Li^+-ion intercalation than a plain thin-film structure. Figure 6 also includes a Ragone plot of specific energy and specific power of various nanostructured vanadium oxide electrodes and an SEM image of typical nanorod arrays.

$LiFePO_4$ demonstrates a high energy density and excellent electrochemical stability. Additional advantages in low cost, low environmental impact, and safety have made the olivine structure a promising cathode material, in particular for large-scale transportation applications. Nonetheless, $LiFePO_4$ has some inherent shortcomings, including one-dimensional Li-ion transport and a two-phase redox reaction that limits the mobility of the phase boundary.[213–216] Thus, nanostructuring has become the key to enable fast rate behavior. Delacourt et al.[216] studied carbon-free $LiFePO_4$ crystalline powders with a narrow distribution around 140 nm, which demonstrated a capacity of 147 mAh g^{-1} at 5 C rate and no significant drop in capacity after 400 cycles. Work by Meethong et al.[217] indicated that the miscibility gap in undoped $Li_{1-x}FePO_4$ contracted with decreasing particle size in the nanoscale regime, suggesting that the miscibility gap could completely disappear after a critical size. Also, they reported that the kinetic response of the nanoscale olivines may deviate from the simple size-scaling implicit in Fickian diffusion. Choi and Kumta[218] synthesized nanostructured $LiFePO_4$ powder with a particle size distribution of 100–300 nm and a crystallite size of less than 65 nm through sol-gel approaches. The synthesized olivine materials demonstrated capacities of 157 and 123 mAh g^{-1} at discharge rates of 1 C and 10 C, respectively, with less than 0.08% fade rate.

4.4. Electrode Architectures in Li-Ion Batteries

Whereas, as demonstrated, the morphology of nanostructures can be optimized for improved electrochemical performance, the overall architecture is another parameter that can be optimized for further improvement. The nanomaterials synthesized are often non-self-supported, that is, they need to be processed into an electrode film. The non-self-supported nanomaterials must be elaborated into an electrode that maintains diffusion length while providing electrical and mechanical contact through the strain imposed by the electrode reactions. While graphitic additives improve the integrity and performance of the nanomaterial electrode, they may incur new penalties arising from the addition of supplementary interfaces. To preserve the benefits of electrochemistry at the nanoscale and to achieve high rate capabilities, 3D nanoarchitectured electrodes (self-supported) may be needed. Such 3D architectured electrodes integrate electrodes and interconnection or current collecting, minimizing loss of interfacial resistance and improving kinetics. This nanomaterial strategy has been applied for the fabrication of conversion electrode materials, such as CoO. Traditional intercalation reactions proceed with Li-ion insertion (or extraction) from an open host structure and concomitant addition (or removal) of electrons, limiting the capacity to at most one Li ion per 3d metal. In contrast, some interstitial-free 3d metal oxide structures (e.g. CoO, CuO, NiO) that exhibit a rock-salt structure with no empty sites available for Li ions (i.e. unsuitable for intercalation chemistry) have nevertheless been shown to exhibit large, rechargeable capacities that can be as high as 1000 mAh g^{-1}.[219–221] It appears that the reversible electrochemical reaction mechanism of Li with the transition oxide, CoO as an example, entails for the most part a displacive redox reaction [Eq. (1)].

$$CoO + 2\,Li^+ + 2e^{-1} \rightleftharpoons Li_2O + Co \qquad (1)$$

Although the reaction to the right is thermodynamically feasible, the reverse reaction to the left which is electrochemically driven is surprising. Observation of the reverse reaction is accounted for by the introduction of nanostructures, though the mechanistic effects of nanostructures on the reversibility of the conversion reactions are still not clear. One drawback of the conversion reactions is the poor electronic conductivity of the conversion materials. One way to overcome the conductivity limit is to develop a nanoarchitectured 3D electrode that is integrated with a highly conductive substrate, such as a metal. Tarascon and co-workers[221–223] reported that nanostructured Fe_3O_4 fabricated on Cu nanorods using template-assisted growth on a current collector (Figure 7) demonstrated a six-

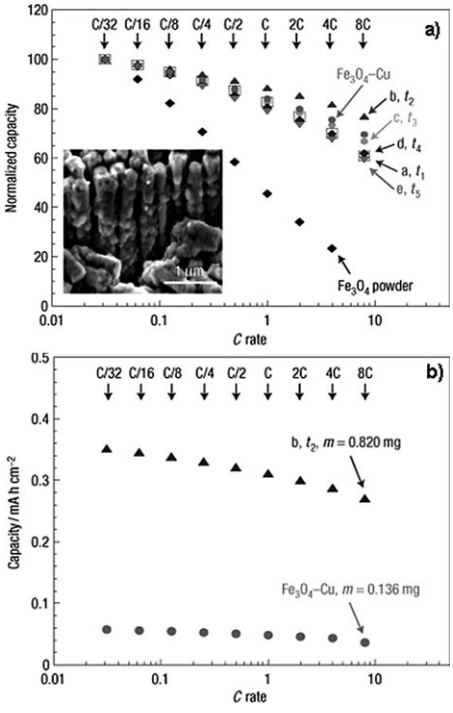

Figure 7. A nanostructured electrode fabricated by electrodeposition of nano-Fe_3O_4 on a nanostructured Cu current collector.[220]

fold improvement in power density over planar electrodes while maintaining the same total discharge time. The capacity at the 8 C rate was 80% of the total capacity and was sustained over 100 cycles. As pointed out by the authors, however, the self-supported material has issues including a large hysteresis between charge and discharge, and the fabrication ap-

proaches need to be optimized so that electrodes with suitable dimensions for practical applications can be produced.

5. Electrical Energy Storage in Supercapacitors

5.1. Introduction

Different from chemical energy storage or batteries that store energy in chemical reactants capable of generating charges, electrochemical capacitors (ECs) store energy directly as charge. There are two types of electrochemical capacitors, namely electrical double-layer capacitors and pseudocapacitors. Recently, high-surface-area carbon has become the leading candidate material for energy storage in electrochemical supercapacitors.[161,224] An electrochemical double-layer capacitor stores electrical energy in the electrochemical double layer formed at the electrode–electrolyte interfacial regions.[225] When the electrode is biased, a double layer structure is developed with the opposite charge accumulated near the electrode surface. The thickness of the double layer is related to the Debye screening length in the modified Gouy–Chapman model. The capacitance (C) of the double layer is related to the surface area (A), the effective dielectric constant or relative permittivity (ε_r), and its thickness (d) by an inverse linear relationship ($C=\varepsilon_r A/d$). A typical smooth surface will have a double-layer capacitance of about 10–20 $\mu F\,cm^{-2}$, but if a high-surface-area electrode surface is used the capacitance can be increased to 100 $F\,g^{-1}$ for a conducting material that has a specific surface area of 1000 $m^2\,g^{-1}$.[162] A wide range of high-surface-area carbon materials have been investigated, including activated carbon and multi- and single-walled carbon nanotubes. The capacitance typically ranges from 40 to 140 $F\,g^{-1}$ for activated carbon,[224] and 15 to 135 $F\,g^{-1}$ for carbon nanotubes.[226,227] Currently, the best available result from commercial products is about 130 $F\,g^{-1}$ (Maxwell's BoostCap). Pseudoelectrochemical capacitance involves voltage-dependent Faradaic reactions between the electrode and the electrolyte, either in the form of surface adsorption/desorption of ions, redox reactions with the electrolyte, or doping/undoping of the electrode materials. The best example of redox pseudocapacitance is hydrous RuO_2, which shows a continuous redox activity over a wide voltage range and very high, surface-area-independent capacitance.[228–231] However, RuO_2 is a very expensive material of limited supply. Much work has been focused on replacing RuO_2 with other metal oxides[232] and nitrides.[233–236] Doped conducting polymers can also display high capacitance, but the stability of the organic materials has so far limited their applications.

Supercapacitors based on carbon materials have been the subject of several excellent reviews; see Ref. [224] for an example. There are several approaches to improve charge storage in carbon supercapacitors. A higher capacitance can be achieved by careful thermal, chemical, or electrochemical treatment to increase the accessible surface area and surface functional groups, or by extending the operating voltage range beyond the limit of an aqueous electrolyte solution.[224] Several critical factors contribute to a high capacitance. First, increasing the surface area is quite important, but significant effort has already been made to maximize the surface area of carbon and there is only limited room for further improvement from the aspect of surface area. For many high-surface-area materials, the correlation between the surface area and the specific capacitance cannot be strictly established.[224] Second, surface functionalization has proven to be effective in increasing the pesudocapacitance arising from oxidation/reduction of surface quindoidal functional groups generated during the treatment of the sample.[237,238] Another widely investigated method to enhance the performance is to coat the carbon materials with redox-active metal oxides such as manganese oxides or conducting polymers such as polyaniline and polypyrrole.[239–241] For example, polypyrrole-coated carbon nanotubes can attain a capacitance of 170 $F\,g^{-1}$,[242] and MnO_2-coated carbon nanotubes can attain a capacitance of 140 $F\,g^{-1}$,[243–245] but these composite materials still do not resolve the fundamental limitations of the polymer and MnO_2, which themselves display limited stability or operating voltage ranges.

5.2. Nanoporous Carbon

One of the most critical requirements is the optimization of the microstructures of the carbon materials. For example, nanostructured porous carbon electrodes with carefully controlled surface chemistry and tuned microporous and mesoporous structures have recently been fabricated by means of sol-gel processing using resorcinol and formaldehyde as precursors, followed by aging, solvent exchange after gelation, removal of the solvent by freeze-drying, and finally pyrolyzing to remove hydrogen and oxygen from the carbon gel at around 1050 °C in nitrogen.[300,301] The resultant porous carbon is referred to as a carbon cryogel, which is similar to the carbon aerogel that is fabricated using supercritical drying. The microporous structure, electrochemical properties, and energy-storage performance are all controlled by the fabrication conditions. The specific capacitance critically depends on the microstructure of the carbon, including the surface area and pore size distribution.[302,303]

Chemical modification of carbon cryogels is used as an efficient approach to alter both the porous structure and surface chemistry, which result in much improved electrochemical properties. Preliminary experiments involved the transportation of ammonia–borane (NH_3BH_3), dissolved in anhydrous THF, to the pores of resorcinol–formaldehyde hydrogels during post-gelation solvent exchange. After being soaked in the NH_3BH_3 solution, the modified hydrogels were subjected to the same freeze-drying and pyrolysis processes as unmodified hydrogels. The resultant modified carbon cryogels are referred to as ABCC, indicating that the samples were modified with ammonia borane as precursor although they are in fact co-doped with boron and nitrogen, whereas the unmodified carbon cryogels are referred to as CC samples. Figure 8a, b compare the typical SEM images of CC and ABCC samples, respectively. The inserts in the top-right corners are high-magnification SEM images, which reveal the highly nanoporous structure in both

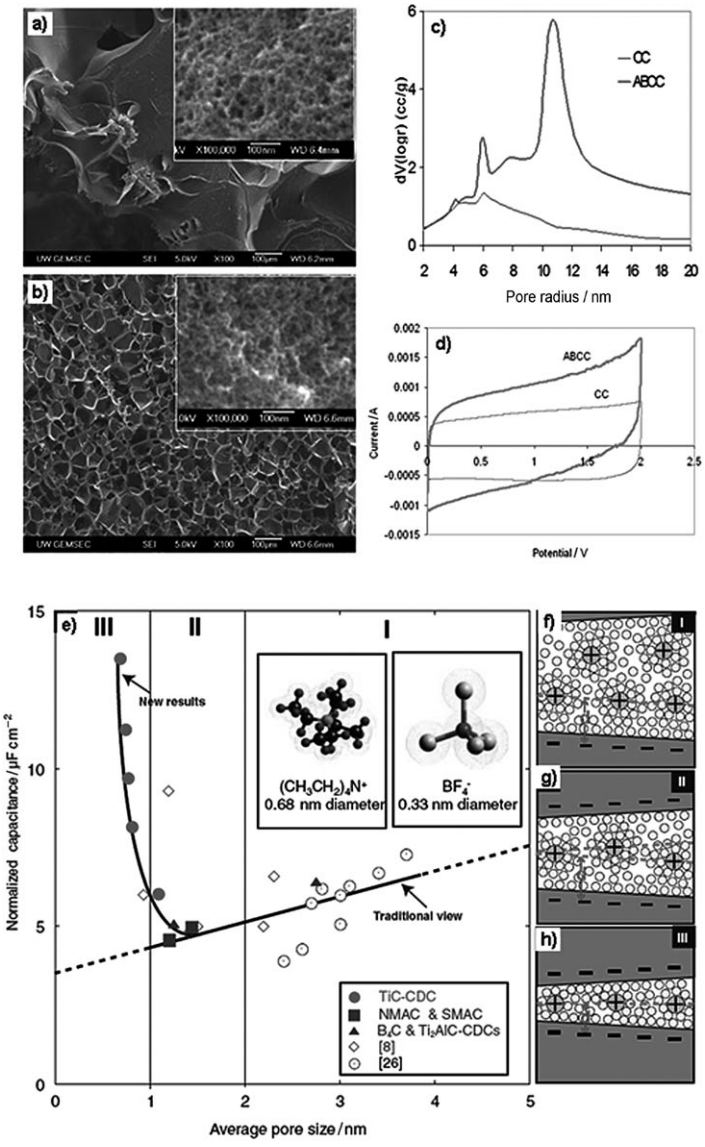

Figure 8. a–d) Microstructure effect of chemically treated carbon crygels (CCs). a) SEM images of a CC. b) SEM image of the ABCC sample (the insets show high-magnification SEM images). c) Comparison of pore size distribution of CC and ABCC samples. d) *C–V* curves for CC and ABCC samples. e–h) Effect of pore sizes on charge storage in carbide-derived carbon materials (see text for details).[246]

samples; however, the relatively low-magnification SEM images differ greatly.

From the SEM images, it is evident that the ABCC sample exhibits a rather uniform macroporous structure whereas the CC sample displays negligible macroporous features under low magnification. Such a difference in porous structure is verified by the pore size distributions derived from the nitrogen-sorption isotherms shown in Figure 8c. ABCC comprises a mixture of much larger pores (>5 nm), which, thereby, result in an increase in pore volume, and a similar number of smaller pores (<5 nm) as CC samples. The voltammogrammic *C–V* curves of ABCC and CC samples (Figure 8d) indicate improved electrochemical properties when the carbon cryogels are co-doped with boron and nitrogen. These improvements in electrical and electrochemical properties are expected, in turn, to lead to significant improvements in energy storage efficiency in both supercapacitors and hybrid batteries.

Interconnected mesoscale porosity plays an important role in ensuring that charged ions can freely access all the surfaces (2–50 nm). Many groups have thus investigated surfactant-templated mesoporous carbon with controllable pore sizes. However, recently, a new study reported the effect of pore size on the charge-storage properties and provided new information on the relative roles of mesoscale and microscale porosity.[246] The charge storage in carbide-derived carbon by high-temperature chloration is reported in Figure 8e–h. This material displays good control of the pore sizes down to less than 1 nm. Three regions are observed: In region I, where the mesopore dominates, the capacitance increases with the pore sizes owing to better pore accessibility and less overlapping of the double layer structure. However, as the pore size becomes smaller in region II, the capacitance begins to increase. In region III, the capacitance increases sharply with decreasing pore sizes. The effect of the ultrasmall pore on the capacitance is attributed to the distortion of the double layers in the small pores and to the decrease in the double layer thickness.

5.3. Oriented Nanostructures

The main advantage of oriented carbon nanotubes is their excellent mechanical properties, electronic conductivity, and more importantly, good ion conduction owing to straight conduction pathways.[247] Futaba et al. prepared free-standing, "solid" dense carbon materials by fluid-drying techniques using long single-walled carbon nanotubes (Figure 9a, b).[247] Even though the specific capacitance is not very impressive ($14\ F\,g^{-1}$), the high power (high current) discharging property is excellent. In comparison, in traditional high-surface-area carbon, the diffusion pathway for the ions is tortuous (Figure 9d). At high currents, the inner surface accessibility is limited and results in a high resistance and loss of capacitance for thick samples.

In another example to illustrate the benefit of oriented nanostructures, Zhou and co-workers[249] recently reported that the specific capacitance of polyaniline films can be increased from around $150\ F\,g^{-1}$ to over $500\ F\,g^{-1}$ using oriented polyaniline nanowires produced by a stepwise method.[38,39] This remarkable increase was attributed to a high surface area and the easy access of the electrolyte through the mesopores in the films made of oriented nanowires. Nanowires of polyaniline, polypyrrole, manganese oxides, and ruthenium oxide usually show a large increase in charge storage.[250–260] Xia and coworkers deposited polyaniline whiskers on ordered mesoporous carbon.[248] The carbon provides good electron conductivity, while the polyaniline whiskers ensure a fast and a short distance of diffusion for the ions. An extremely high capacitance of over $700\ F\,g^{-1}$ (over $1000\ F\,g^{-1}$ if just the polymer was counted) was observed for the composite material even at a high current density, with minimum capacitance loss over long cycles.

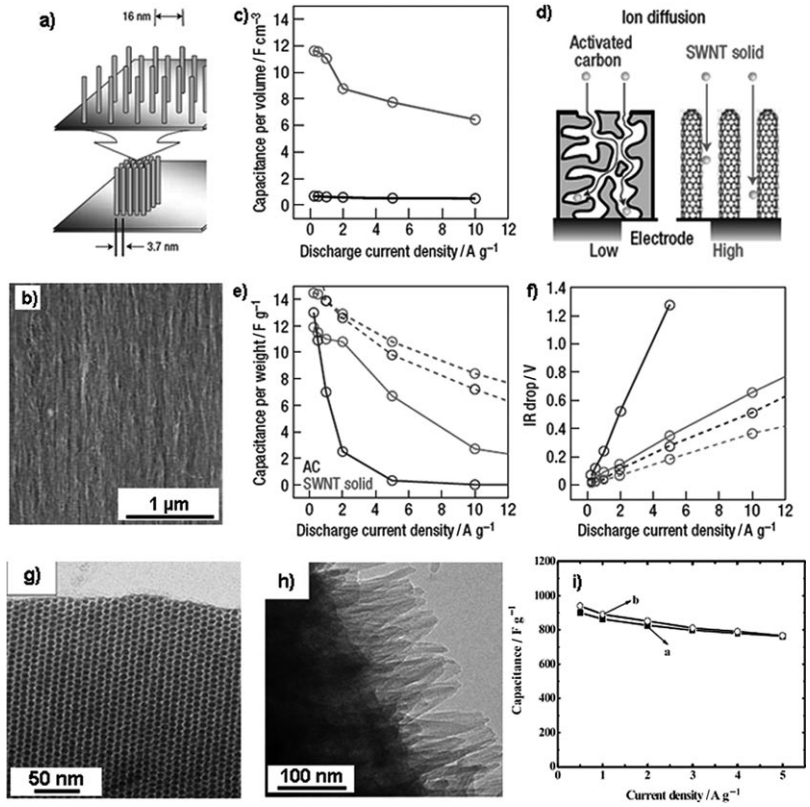

Figure 9. Comparison of activated carbon and oriented carbon nanotubes. a) Fluid drying to form dense solid carbon from long single-walled carbon nanotubes (SWCNTs). b) TEM image of the nanotube solid. c) Capacitance per volume for dried (pale gray line) and as-prepared (dark gray line) SWCNTs. d) Ion diffusion in activated carbon and oriented CNTs. e) Specific capacitance as a function of current density (CNTS pale gray line, activated carbon dark gray line). f) Potential drop as a function of current density.[247] g,h) Polyaniline whisker coated mesoporous carbon:[248] TEM images of the mesoporous carbon (g) and polyaniline whiskers on carbon (h). i) Capacitance as a function of current density.

6. Nanostructured Thermoelectrics

6.1. Introduction

The primary mode for power generation worldwide entails burning fossil fuels and converting the energy released, which involves the generation of heat. Much of the heat, however, is wasted in this process without being converted into electricity. The conversion of thermal energy to electricity (the Seebeck effect) or vice versa (the Peltier effect) can be accomplished using p–n junctions made of thermoelectric materials (Figure 10 a, b).[261] Thermoelectric devices have a wide range of applications such as more effective removal of heat from integrated circuits, cooling laser diodes, and ultimately refrigerator, air conditioners, and portable devices for cooling. Despite the advantages that thermoelectric devices offer, the use of such devices is limited primarily because of their low efficiencies.

The efficiency of thermoelectric materials and devices is determined by the non-dimensional figure of merit, $ZT = \sigma S^2 T/k$ (S is the Seebeck coefficient, σ is the electrical conductivity, k is the thermal conductivity, and T is the absolute temperature). The progress made between the 1960s and the 1990s in improving the ZT value was very slow. Currently, the state-of-the-art thermoelectric material is a bulk Bi_2Te_3-based alloy with a ZT value of around unity. The long-sought goal for ZT values is around 3. Most recently, a set of new thermoelectric materials with high ZT values (>1) have been developed through electron and phonon engineering using nanostructures.[26–28] Table 1 compares the power factor σS^2 and thermal conductivity of the two reported high-ZT thermoelectric material systems. There is a small change in the power factor, while the thermal conductivities of the structures are significantly reduced. Extensive research in thermoelectric properties of superlattices and one-dimensional nanostructures has shown that ZT enhancement comes mainly from the reduction in thermal conductivity owing to incoherent phonon scattering at the interface while concurrently improving or maintaining electron performance.[262] Clearly, nanoporous and/or nanocomposite thermoelectrics offer great potential for fabricating low-cost, high-efficiency thermoelectric devices.

6.2. Oriented Nanowires

One-dimensional materials provide the opportunity to independently optimize S, σ, and k, which is difficult in bulk materials. A high ZT value is predicted in the one-dimensional materials as a result of the enhanced charge mobility arising from the quantum confinement of the density of states and reduced phonon transport owing to the boundary scattering effect (reduced thermal conductivity),[77,263] but the fabrication of nanowire-based thermoelectric devices remains a great challenge. Nanowire and nanorod arrays of thermoelectric semiconductors have been synthesized using anodic alumina membrane (AAM) templates. Nanowire arrays of bismuth telluride (Bi_2Te_3) are a good example to illustrate the synthesis of compound nanowire arrays by electrochemical deposition using AAM templates. Bi_2Te_3 is of special interest as a thermoelectric material, and Bi_2Te_3 nanowire arrays are believed to offer a higher figure of merit for thermal–electrical energy conversion.[77,78] Both polycrystalline and single-crystal Bi_2Te_3 nanowire arrays have been grown by electrochemical deposition inside anodic alumina membranes.[79,80] Sander and co-workers[79,80,264] fabricated Bi_2Te_3 nanowire arrays with diameters as small as about 25 nm from a solution of 0.075 M Bi and 0.1 M Te in 1 M HNO_3 by electrochemical deposition at -0.46 V (vs Hg/Hg_2SO_4 reference

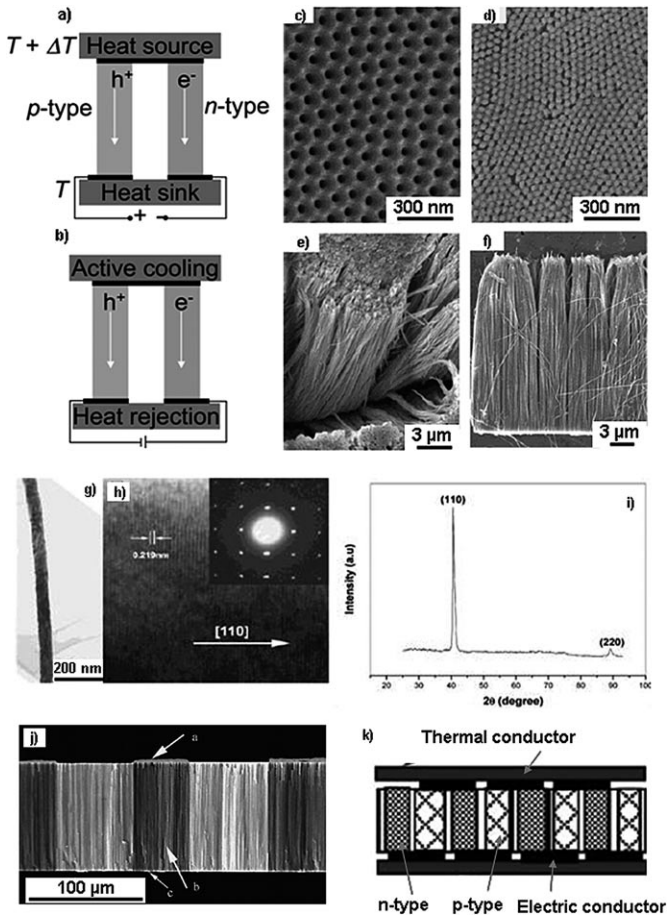

Figure 10. a, b) Schematic of thermoelectric devices. The semiconductors between the thermal terminals can be oriented nanowires. c–i) SEM and TEM photographs and XRD patterns of the AAM template and Bi_2Te_3 nanowire arrays: c) a typical SEM image of AAM; d) surface view of Bi_2Te_3 nanowire arrays (eroding time: 5 min); e) surface view of Bi_2Te_3 nanowire arrays (eroding time: 15 min); f) cross-sectional view of Bi_2Te_3 nanowire arrays (eroding time: 15 min);[80] g) TEM image of the nanowires; h) high-resolution TEM image of the same nanowires (the inset shows the corresponding electron diffraction pattern); i) XRD pattern of Bi_2Te_3 nanowire arrays (electrodeposition time: 5 min).[267] j) Micropatterned Bi_2Te_3 nanowires for the microthermoelectric devices based on alumina template. k) A proposed four-layer microthermoelectric device.[267]

Table 1. Properties of selected thermoelectric materials with high *ZT* values.[26,27]

Sample[a]	Thermoelectric properties (300 K)		
	$S^2\sigma$ [mW cm^{-1} K^{-2}]	k [W m^{-1} K^{-1}]	ZT
PbTe-PbSeTe QD SLs	32	0.6	1.6
PbTe-PbSeTe bulk alloy	28	2.5	0.34
Bi_2Te_3-Sb_2Te_3 SLs	40	0.5	2.4
Bi_2Te_3-Sb_2Te_3 bulk alloy	50	1.45	1.0

[a] QD = quantum dot; SL = superlattice.

electrode). The resultant Bi_2Te_3 nanowire arrays are polycrystalline in nature, and subsequent melting–recrystallization failed to produce single-crystal Bi_2Te_3 nanowires. However, single-crystal Bi_2Te_3 nanowire arrays have been electrochemically grown from a solution of 0.035 M $Bi(NO_3)_3{\cdot}5H_2O$ and 0.05 M $HTeO_2^+$ prepared by dissolving Te powder in 5 M HNO_3.[80] Figure 10c–i present SEM and TEM images along with XRD patterns showing the cross-section of Bi_2Te_3 nanowire arrays and their crystal orientation. High-resolution TEM and electron diffraction studies, together with XRD revealed that the preferred growth direction of Bi_2Te_3 nanowires is the [110] direction. Single-crystal nanowire or nanorod arrays can also be made through a careful control of the initial deposition.[265] Similarly, large-area Sb_2Te_3 nanowire arrays have also been successfully grown by template-based electrochemical deposition, but the grown nanowires are polycrystalline and show no clear preferred growth direction.[266]

Actual fabrication of thermoelectric micro- or nanodevices from nanowires remains challenging. Dresselhaus and co-workers measured the thermoelectric properties of both single nanowires and nanowire arrays.[268] The temperature dependence of the resistivity in the nanowire is different from the semimetallic behavior of the bulk material, but only a very small fraction of the nanowires contribute to the conducitivity. Lim et al. proposed a microarray by first electrochemically depositing n-type Bi_2Te_3 nanowires in micropatterned alumina templates, followed by electrochemical deposition of p-type BiSbTe (Figure 10j).[269] The thermoelectric devices would be made of interconnected p–n junctions in a serial arrangement. Wang et al. discussed a similar four-layer microthermoelectric device made of p-type and n-type Bi_2Te_3 nanowires sandwiched between an electrical conductor and a Si thermal conductor layer (Figure 10k).[267] The Seebeck coefficients of the n-type and p-type Be_2Te_3 nanowires were measured to be 260 and -188 mV K^{-1}, respectively, but the actual device and its performance were not reported.

So far, the greatest benefit from one-dimensional materials is the reduction in thermal conductivity.[271] Recently, Hochbaum et al. carried out a fundamental study of Si nanowires by electroless etching methods.[270] As compared to commonly investigated Bi-based semiconductors that are expensive to manufacture, Si is already widely used in the microelectronics industry. The microstructure and thermal conductivity of Si nanowires prepared by VLS methods and electroless etching methods were compared. The Si nanowires obtained by electroless etching varied from 20 to 300 nm in diameter and 5 to 150 μm in length, but unlike the Si nanowires from the VSL method which display smooth surfaces, the electroless etching Si nanowires have enhanced surface roughness (Figure 11). Their thermal conductivity is much lower than bulk Si and Si nanowires obtained from VLS methods and approaches that of amorphous Si. As the reduced thermal conductivity cannot merely be explained by the size effect of the nanowires owing to boundary scattering from the surface, surface roughness is believed to be the main reason for this unusual property. As a result, the Si nanowires obtained by electroless etching can achieve a figure of merit (*ZT*) of 0.6 at room temperature, orders of magnitude higher than that for bulk Si materials. Recently, Heath and co-workers developed a four-point measurement platform to study the thermoelectric properties of Si nanowires prepared from a supperlattice nanowire pattern

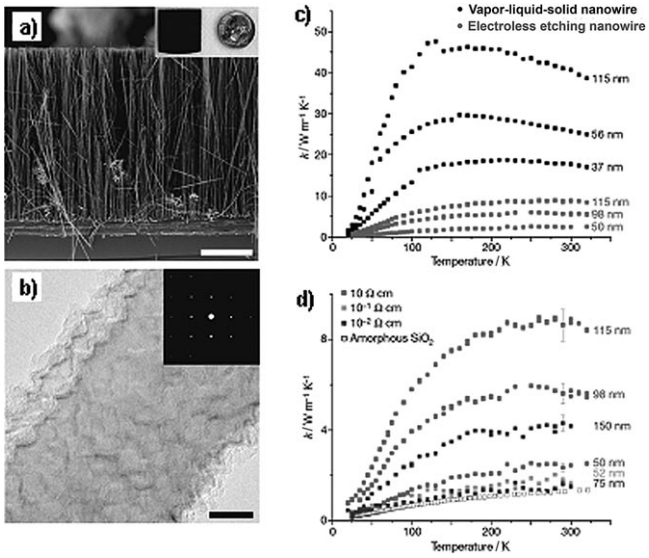

Figure 11. Potential of electroless etching Si nanowires for thermoelectrics.[270] a) SEM image of the oriented nanowires. b) TEM image of the nanowire with rough surface. c) Comparison of thermal conductivity of VSL nanowires (black) and electroless etching nanowires (gray). d) Thermal conductivity of electroless etching nanowires of different resistivity.

transfer (SNAP) method.[272] This method retains the intrinsic doping level in the single-crystal Si substrate. By varying the doping level and the nanowire dimension, *ZT* values increased by two orders of magnitude, approaching unity at 200 K. This increased efficiency was attributed to the phonon effect. Previously, four-point measurements were conducted on polycrystalline Bi nanowires.[273] Bi has a small effective mass, large thermoelectric power, and low thermal conductivity, but in Bi nanowires the contributions from electrons and holes cancel each other owing to the semimetallic nature of the materials.

7. Future Perspectives

One grand challenge in energy conversion and storage is to master the energy and information on the nanoscale to create materials and technologies with capabilities rivaling those of living systems.[274] A large portion of this Review has discussed the importance of transport phenomena and the access of a nanoconfined environment for energy conversion and storage. For other applications such as proton-exchange membrane fuel cells, batteries, and capacitors, effective ion transport is also critical for their performance.[275–279] In biology, cells developed very sophisticated protein channels to transport fluid and ions across cell membranes, and the identification of the structure and function of such channels was hailed as some of the greatest scientific discoveries.[280] For example, proton transport through transmembrane proton channels can be 15 times faster than that of other ions (K^+) and 8 times faster than that of the water molecule.[281] Although the details differ from different simulations, it was demonstrated that the faster proton transport was achieved through a fast diffusion mechanism along single water molecular wires.[282–284] On the other hand, in biological water channels, only water molecules are allowed to go through partially because of the positive charge in the channels (Figure 12a).[285] Selective cation diffusion in ion channels is accomplished by structural matching of the coordinates with the cations.[286] Unusual proton conductivity was also found in very narrow hydrophobic channels.[287] These results suggest that selective and effective transport can be achieved during materials synthesis by precisely designed nanochannels through rational consideration of the interfacial interactions, channel sizes, and molecular and nanoscale structural refinement. Several groups have begun to investigate water diffusion in hydrophobic carbon nanotubes.[288,289] Another material candidate to understand and optimize the fundamental transport properties could be the self-assembled nanoarrays and nanochannels discussed earlier (Section 2.5.).[86,87,290] In such nanochannels, the surface chemistry, the pore dimension, and the molecular and nanoscale ordering can be systematically adjusted (Figure 12b).[291,292]

Besides ion channels, biological molecular machines contain highly integrated structures and functions. An examination of biological catalysts such as the hydrogenase enzyme (Figure 12c) illustrates features that are common to biological systems for energy-conversion processes.[293,294] This enzyme requires channels for conducting electrons and protons to and from the catalytically active sites. In addition, the enzyme has a channel for the transport of H_2. This organized architecture requires the transport of electrons, protons, and hydrogen over nanoscale dimensions and an intersection of all three channels at the molecular scale. This highly structured assembly from the molecular to the nanometer scale is important for the overall efficiency of the enzyme. The proton and electron transport must occur over micro- to nanoscale dimensions, and these pathways must be coupled on a molecular scale with the catalytically active site. These enzyme structures suggest that controlling proton and electron flows over large distances and precisely controlling the intersection of these channels with the catalytically active site is crucial to the development of highly efficient systems for interconverting between electrical energy and fuels, that is, fuel cells and solar cell devices.

Integration of materials and functions to achieve performance that is not possible with individual components is one of the most significant challenges in energy conversion and storage. At the nano- and micrometer scales, on-board energy harvesting, conversion, and storage not only play an important role in remote sensing and manipulation and a whole range of electronic and optical devices but it may also lead to drastically different approaches for large-scale energy conversion and storage. Recently, several groups have demonstrated novel methods to integrate oriented nanostructures with energy-conversion mechanisms. In the first example, Wang and Song reported an important breakthrough in piezoelectric nanogenerators based on ZnO nanowire arrays.[295] In this landmark study, [0001]-oriented ZnO nanowire arrays were grown on α-Al_2O_3 substrates. The ZnO nanowires were deflected by a conductive atomic force microscope (AFM) tip (Figure 13, left panel). This deformation produced coupled piezoelectric and semiconducting responses in the ZnO material. The bending

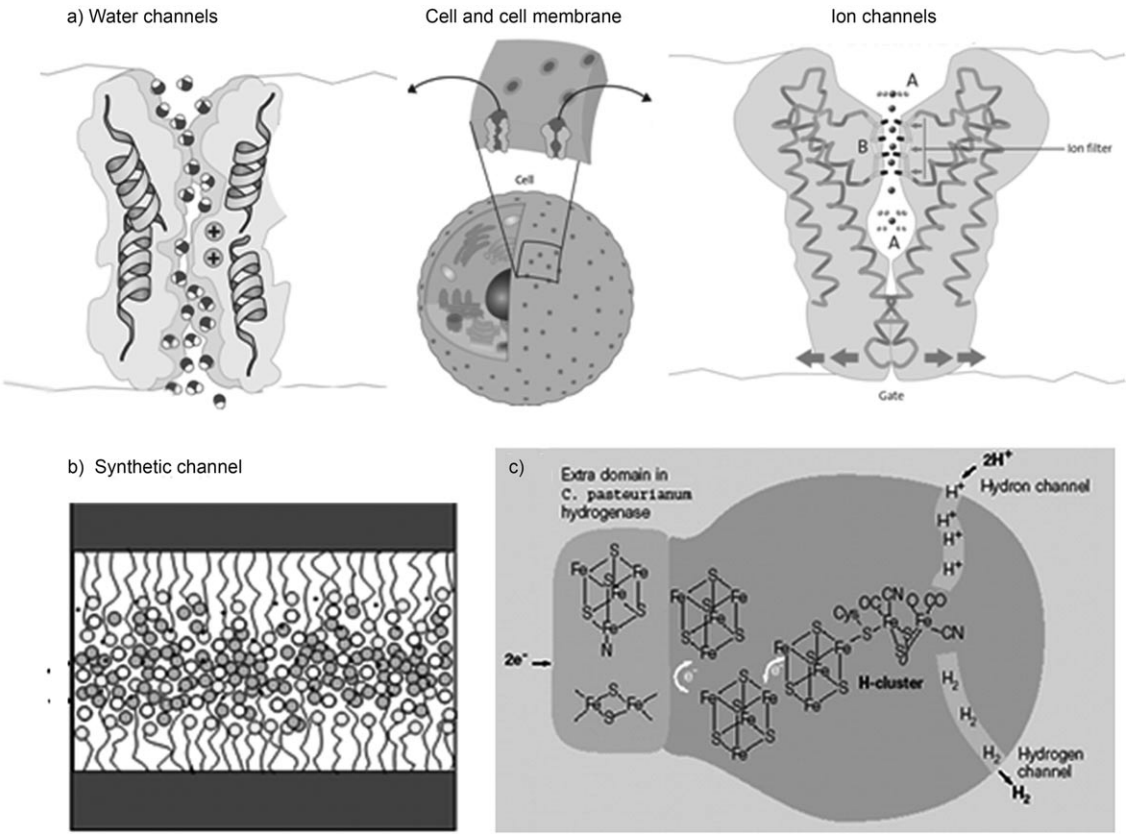

Figure 12. a) Schematic illustration of water and potassium channels in cell membranes.[285] b) A conceptual artificial proton channel based on self-assembled nanoporous channels. c) Illustration of the structure of a hydrogenase enzyme molecule.

and strain field resulted in a charge separation, which was detected as electrical currents in the AFM tip. Nanogenerators based on the piezoelectric properties of ZnO arrays are expected to have potential for powering remote sensors, biomedical devices, and many other optoelectronic devices because many different kinds of mechanical energy can be used to generate electricity. Although in the AFM-based device the power generation efficiency can be as high as 17–30%, the manufacture and operation of the device are challenging. To solve these problems, Wang and co-workers replaced the AFM tip with a saw-shaped zigzag Si electrode (Figure 13, right panel).[296] They then further fabricated nanowire functionalized microfibers for energy scavenging.[297] The new device became much more practical and also increased the total current that could be generated.

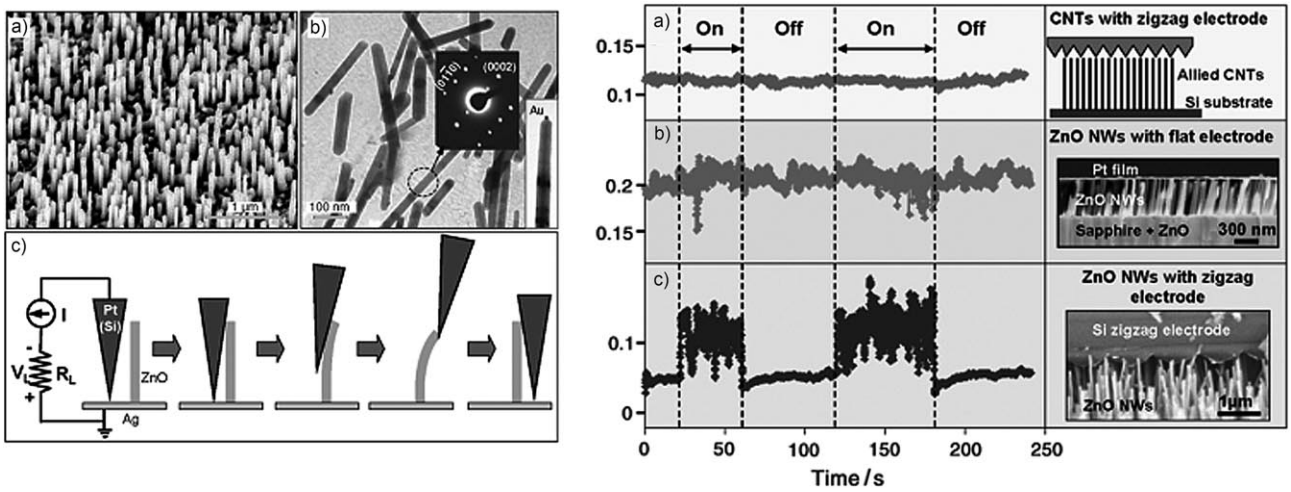

Figure 13. Converting mechanical energy into electricity using ZnO nanoarrays. Left panel: electricity generated by AFM tips. Right panel: electricity generated by saw-shaped Si electrodes. Note that the electricity was only generated with ZnO using the zigzag Si electrode.[295,296]

In the second example, Lieber and co-workers fabricated coaxial p-type-intrinsic-n-type (p-i-n) Si photovoltaic devices that demonstrated a maximum output power of 200 pW and energy-conversion efficiencies of 3.4%.[298] A single nanowire photovoltaic element was integrated with a sensing device and provided sufficient power to drive the sensor.

On the grand scale, there are two aspects of the energy problem: the increasing global demand and the increasing levels of greenhouse emissions. The need to simultaneously increase our energy supply while reducing CO_2 emissions is one of the major challenges facing our global society today. Future energy sources that can meet these dual requirements include solar, wind, and nuclear energy—all of which produce electricity as the primary form of energy. The conversion of this energy to fuels such as methanol or hydrogen using common substrates such as CO_2 and water provides an opportunity to remove the temporal variation in the energy supply from solar and wind energy sources and to integrate these energy sources with each other and with fossil energy. Such integration would allow an orderly transition from current fossil-based energy supplies to future non-fossil energy sources. In addition, the direct conversion of fuels into electrical energy is known to be potentially much more efficient than internal combustion engines. As a result, the development of new materials that will permit the efficient conversion of electricity into fuels and the reverse, fuels into electricity, will be important in meeting the future energy needs of our society.

From a materials perspective, the question is what materials and functions are needed to address such complicated energy-conversion problems. To gain some perspective on this issue, we can consider a membrane for artificial photosynthesis and an enzyme for H_2 production/oxidation. A schematic diagram of an artificial photosynthetic membrane is shown in Figure 14, which illustrates the essential features of an idealized integrated system for solar conversion of CO_2 into methanol. In this schematic, light absorption and charge separation occur at the semiconductor, the light-harvesting component. The charge separation requires the movement of electrons or holes over a significant distance. Accompanying this movement of electrons is the movement of protons from one side of the membrane to another. There are also two catalytic half-reactions. On the CO_2 reduction side, the catalyst accepts six electrons from the semiconductor surface and combines these electrons with six protons (from a proton-conduction pathway) and CO_2 to produce methanol [Eq. (2)]. On the H_2O oxidation side, the catalyst mediates the oxidation of two water molecules to produce O_2 and four protons [Eq. (3)]. This membrane represents a highly integrated system for the solar production of a fuel that involves the precise organization of the components required for charge separation, proton transport, and catalysis.

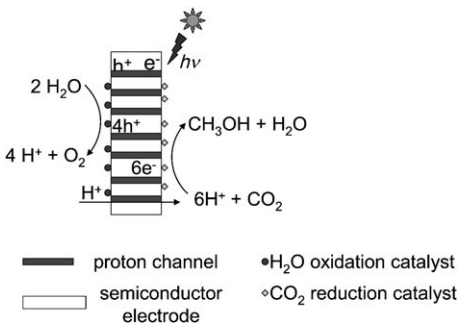

Figure 14. Schematic of a bio-inspired membrane for artificial photosynthesis.

$$6e^- + 6H^+ \rightarrow CH_3OH + H_2O \quad (2)$$

$$2H_2O \rightarrow 4H^+ + O_2 + 4e^- \quad (3)$$

The examples cited above highlight the challenges in materials science in the conversion of electrical and chemical energy, that is, discovery of novel electronic and electrochemically active materials, multiscale assembly and integration of molecular species with nano- and macroscale materials, coupling of molecular chemistry with materials sciences, optimizing the transport of electrons and protons over required distances, and spatial positioning and distribution of components and functionalities. In this particular case, both the properties of the materials (proton-conducting channels, wires for electron transfer, and catalytically active sites) and their organizations have to be correct. New approaches have to involve a shift in materials science from one of obtaining a single material with optimal properties to one of precisely assembled multicomponent materials composed of designed functional materials (for electron and proton transport and catalysis) that are integrated across a range of scales from the size of individual molecules through nanoscopic and microsopic scales to macrosopic devices.

Acknowledgements

The work performed at the Pacific Northwest National Laboratory (PNNL) was supported by the Laboratory-Directed Research and Development Program of the Pacific Northwest National Laboratory and by the Office of Basic Energy Sciences, U.S. Department of Energy (DOE). PNNL is a multiprogram laboratory operated by the Battelle Memorial Institute for the Department of Energy under contract DE-AC05-76 L01830. The work at the University of Washington was supported in part by the National Science Foundation (DMI-0455994 and DMR-0605159), Air Force Office of Scientific Research (AFOSR-MURI, FA9550-06-1-032), Department of Energy (DE-FG02-07ER46467), Washington Technology Center, Washington Research Foundation, and EnerG2, LLC.

Keywords: energy conversion · energy storage · materials science · nanostructures

[1] R. E. Smalley, *MRS Bull.* **2005**, *30*, 412.
[2] US DOE Office of Basic Energy Sciences, *Basic Energy Needs for Solar Energy Utilization: Report of the Basic Energy Sciences Workshop on Solar Energy Utilization*, **2006**.
[3] B. T. Holland, C. F. Blanford, T. Do, A. Stein, *Chem. Mater.* **1999**, *11*, 795.
[4] R. Heinberg, *Energy Bulletin* **2007**; http://www.energybulletin.net/node/29919.

[5] P. Norling, F. Wood-Black, T. M. Masciangioli, *Water and Sustainable Development: Opportunities for the Chemical Sciences—A Workshop Report to the Chemical Sciences Roundtable*, National Academies Press, **2004**.
[6] A. O. Converse, *Appl. Biochem. Biotech.* **2007**, *137*, 611.
[7] E. J. Jacob, *Curr. Sci.* **2007**, *92*.
[8] K. L. W. Shum, C. Watanabe, *Energy Policy* **2007**, *35*, 1186.
[9] P. D. Lund, *Renewable Energy* **2007**, *32*, 442.
[10] W. Hoffmann, *Sol. Energy Mater. Sol. Cells* **2006**, *90*, 3285.
[11] R. Gross, M. Leach, A. Bauen, *Environ. Int.* **2003**, *29*, 105.
[12] A. H. S. Luque *Handbook of Photovoltaic Science and Engineering*; John Wiley & Sons Ltd, New York, **2003**.
[13] J. Merrill, D. C. Senft, *JOM* **2007**, *59*, 26.
[14] A. D. Compaan, *JOM* **2007**, *59*, 31.
[15] L. L. Kazmerski, *J. Electron Spectrosc. Relat. Phenom.* **2006**, *150*, 105.
[16] M. M. Alam, S. A. Jenekhe, *Chem. Mater.* **2004**, *16*, 4647.
[17] B. A. Gregg, *J. Phys. Chem. B* **2003**, *107*, 4688.
[18] P. Peumans, S. Uchida, S. R. Forrest, *Nature* **2003**, *425*, 158.
[19] P. Peumans, A. Yakimov, S. R. Forrest, *J. Appl. Phys.* **2003**, *93*, 3693.
[20] S. E. Shaheen, R. Radspinner, N. Peyghambarian, G. E. Jabbour, *Appl. Phys. Lett.* **2001**, *79*, 2996.
[21] G. Dennler, N. S. Sariciftci, *Proc. IEEE* **2005**, *93*, 1429.
[22] S. A. Jenekhe, S. J. Yi, *Appl. Phys. Lett.* **2000**, *77*, 2635.
[23] M. M. Alam, S. A. Jenekhe, *J. Phys. Chem. B* **2001**, *105*, 2479.
[24] J. G. Xue, B. P. Rand, S. Uchida, S. R. Forrest, *Adv. Mater.* **2005**, *17*, 66.
[25] R. W. Miles, G. Zoppi, I. Forbes, *Mater. Today* **2007**, *10*, 20.
[26] T. C. Harman, P. J. Taylor, M. P. Walsh, B. E. LaForge, *Science* **2002**, *297*, 2229.
[27] R. Venkatasubramanian, E. Siivola, T. Colpitts, B. O'Quinn, *Nature* **2001**, *413*, 597.
[28] K. F. Hsu, S. Loo, F. Guo, W. Chen, J. S. Dyck, C. Uher, T. Hogan, E. K. Polychroniadis, M. G. Kanatzidis, *Science* **2004**, *303*, 818.
[29] S. F. J. Flipsen, *J. Power Sources* **2006**, *162*, 927.
[30] C. K. Dyer, *IEEE—2004 Symposium on VLSI Circuits, Digest of Technical Papers*, **2004**, 124.
[31] S. Yae, T. Kobayashi, M. Abe, N. Nasu, N. Fukumuro, S. Ogawa, N. Yoshida, S. Nonomura, Y. Nakato, H. Matsuda, *Sol. Energy Mater. Sol. Cells* **2007**, *91*, 224.
[32] S. S. Mao, X. B. Chen, *Int. J. Energy Res.* **2007**, *31*, 619.
[33] A. S. Arico, P. Bruce, B. Scrosati, J. M. Tarascon, W. Van Schalkwijk, *Nat. Mater.* **2005**, *4*, 366.
[34] J. Maier, *Nat. Mater.* **2005**, *4*, 805.
[35] C. J. Brinker, *Sol-Gel Science: The Physics and Chemistry of Sol-Gel Processing*, Academic Press, Inc., San Diego, **1990**.
[36] B. O'Regan, M. Grätzel, *Nature* **1991**, *353*, 737.
[37] H. D. Gesser, P. C. Goswami, *Chem. Rev.* **1989**, *89*, 765.
[38] L. Liang, J. Liu, C. F. Windisch, G. J. Exarhos, Y. H. Lin, *Angew. Chem.* **2002**, *114*, 3817; *Angew. Chem. Int. Ed.* **2002**, *41*, 3665.
[39] J. Liu, Y. H. Lin, L. Liang, J. A. Voigt, D. L. Huber, Z. R. Tian, E. Coker, B. McKenzie, M. J. McDermott, *Chem. Eur. J.* **2003**, *9*, 604.
[40] G. K. Mor, K. Shankar, M. Paulose, O. K. Varghese, C. A. Grimes, *Nano Lett.* **2006**, *6*, 215.
[41] M. Zukalova, A. Zukal, L. Kavan, M. K. Nazeeruddin, P. Liska, M. Graetzel, *Nano Lett.* **2005**, *5*, 1789.
[42] C. D. Liang, K. L. Hong, G. A. Guiochon, J. W. Mays, S. Dai, *Angew. Chem.* **2004**, *116*, 5909; *Angew. Chem. Int. Ed.* **2004**, *43*, 5785.
[43] J. W. P. Hsu, Z. R. Tian, N. C. Simmons, C. M. Matzke, J. A. Voigt, J. Liu, *Nano Lett.* **2005**, *5*, 83.
[44] R. S. Wagner, W. C. Ellis, *Appl. Phys. Lett.* **1964**, *4*, 89.
[45] W. Z. Li, S. S. Xie, L. X. Qian, B. H. Chang, B. S. Zou, W. Y. Zhou, R. A. Zhao, G. Wang, *Science* **1996**, *274*, 1701.
[46] Z. F. Ren, Z. P. Huang, J. W. Xu, J. H. Wang, P. Bush, M. P. Siegal, P. N. Provencio, *Science* **1998**, *282*, 1105.
[47] M. H. Huang, S. Mao, H. Feick, H. Q. Yan, Y. Y. Wu, H. Kind, E. Weber, R. Russo, P. D. Yang, *Science* **2001**, *292*, 1897.
[48] Y. Y. Wu, H. Q. Yan, M. Huang, B. Messer, J. H. Song, P. D. Yang, *Chem. Eur. J.* **2002**, *8*, 1260.
[49] L. Vayssieres, K. Keis, A. Hagfeldt, S. E. Lindquist, *Chem. Mater.* **2001**, *13*, 4395.
[50] L. Vayssieres, K. Keis, S. E. Lindquist, A. Hagfeldt, *J. Phys. Chem. B* **2001**, *105*, 3350.
[51] Z. R. R. Tian, J. A. Voigt, J. Liu, B. McKenzie, M. J. McDermott, *J. Am. Chem. Soc.* **2002**, *124*, 12954.
[52] L. E. Greene, M. Law, J. Goldberger, F. Kim, J. C. Johnson, Y. F. Zhang, R. J. Saykally, P. D. Yang, *Angew. Chem.* **2003**, *115*, 3139; *Angew. Chem. Int. Ed.* **2003**, *42*, 3031.
[53] L. E. Greene, M. Law, D. H. Tan, M. Montano, J. Goldberger, G. Somorjai, P. D. Yang, *Nano Lett.* **2005**, *5*, 1231.
[54] Z. R. R. Tian, J. A. Voigt, J. Liu, B. McKenzie, M. J. McDermott, M. A. Rodriguez, H. Konishi, H. F. Xu, *Nat. Mater.* **2003**, *2*, 821.
[55] D. H. Wang, J. Liu, Q. S. Huo, Z. M. Nie, W. G. Lu, R. E. Williford, Y. B. Jiang, *J. Am. Chem. Soc.* **2006**, *128*, 13670.
[56] T. L. Sounart, J. Liu, J. A. Voigt, M. Huo, E. D. Spoerke, B. McKenzie, *J. Am. Chem. Soc.* **2007**, *129*, 15786.
[57] T. R. Zhang, W. J. Dong, M. Keeter-Brewer, S. Konar, R. N. Njabon, Z. R. Tian, *J. Am. Chem. Soc.* **2006**, *128*, 10960.
[58] T. L. Sounart, J. Liu, J. A. Voigt, J. W. P. Hsu, E. D. Spoerke, Z. Tian, Y. B. Jiang, *Adv. Funct. Mater.* **2006**, *16*, 335.
[59] N. R. Chiou, C. M. Lui, J. J. Guan, L. J. Lee, A. J. Epstein, *Nat. Nanotechnol.* **2007**, *2*, 354.
[60] R. C. Furneaux, W. R. Rigby, A. P. Davidson, *Nature* **1989**, *337*, 147.
[61] R. J. Tonucci, B. L. Justus, A. J. Campillo, C. E. Ford, *Science* **1992**, *258*, 783.
[62] G. E. Possin, *Rev. Sci. Instrum.* **1970**, *41*, 772.
[63] C. G. Wu, T. Bein, *Science* **1994**, *266*, 1013.
[64] D. H. Wang, H. M. Luo, R. Kou, M. P. Gil, S. G. Xiao, V. O. Golub, Z. Z. Yang, C. J. Brinker, Y. F. Lu, *Angew. Chem.* **2004**, *116*, 6295; *Angew. Chem. Int. Ed.* **2004**, *43*, 6169.
[65] D. H. Wang, W. L. Zhou, B. F. McCaughy, J. E. Hampsey, X. L. Ji, Y. B. Jiang, H. F. Xu, J. K. Tang, R. H. Schmehl, C. O'Connor, C. J. Brinker, Y. F. Lu, *Adv. Mater.* **2003**, *15*, 130.
[66] D. H. Wang, H. P. Jakobson, R. Kou, J. Tang, R. Z. Fineman, D. H. Yu, Y. F. Lu, *Chem. Mater.* **2006**, *18*, 4231.
[67] D. H. Wang, R. Kou, M. P. Gil, H. P. Jakobson, J. Tang, D. H. Yu, Y. F. Lu, *J. Nanosci. Nanotechnol.* **2005**, *5*, 1904.
[68] S. S. Fan, M. G. Chapline, N. R. Franklin, T. W. Tombler, A. M. Cassell, H. J. Dai, *Science* **1999**, *283*, 512.
[69] P. Enzel, J. J. Zoller, T. Bein, *J. Chem. Soc. Chem. Commun.* **1992**, 633.
[70] C. Guerret-Piécourt, Y. Lebouar, A. Loiseau, H. Pascard, *Nature* **1994**, *372*, 761.
[71] P. M. Ajayan, O. Stephan, P. Redlich, C. Colliex, *Nature* **1995**, *375*, 564.
[72] A. Despic, V. P. Parkhutik, *Modern Aspects of Electrochemistry, Vol. 20* (Eds.: J. O. M. Bockris, R. E. White, B. E. Canway), Plenum Press, New York, **1989**.
[73] D. Almawlawi, N. Coombs, M. Moskovits, *J. Appl. Phys.* **1991**, *70*, 4421.
[74] D. Almawlawi, N. Coombs, M. Moskovits, *J. Appl. Phys.* **1991**, *69*, 5150.
[75] C. A. Foss, M. J. Tierney, C. R. Martin, *J. Phys. Chem.* **1992**, *96*, 9001.
[76] R. L. Fleischer, P. B. Price, R. M. Walker, *Nuclear Tracks in Solids*, University of California Press, Berkeley, **1975**.
[77] L. D. Hicks, M. S. Dresselhaus, *Phys. Rev. B* **1993**, *47*, 16631.
[78] M. S. Dresselhaus, G. Dresselhaus, X. Sun, Z. Zhang, S. B. Cronin, T. Koga, *Phys. Solid State* **1999**, *41*, 679.
[79] M. S. Sander, R. Gronsky, T. Sands, A. M. Stacy, *Chem. Mater.* **2003**, *15*, 335.
[80] C. G. Jin, X. Q. Xiang, C. Jia, W. F. Liu, W. L. Cai, L. Z. Yao, X. G. Li, *J. Phys. Chem. B* **2004**, *108*, 1844.
[81] M. Paulose, K. Shankar, S. Yoriya, H. E. Prakasam, O. K. Varghese, G. K. Mor, T. A. Latempa, A. Fitzgerald, C. A. Grimes, *J. Phys. Chem. B* **2006**, *110*, 16179.
[82] M. Paulose, H. E. Prakasam, O. K. Varghese, L. Peng, K. C. Popat, G. K. Mor, T. A. Desai, C. A. Grimes, *J. Phys. Chem. C* **2007**, *111*, 14992.
[83] S. Yoriya, H. E. Prakasam, O. K. Varghese, K. Shankar, M. Paulose, G. K. Mor, T. J. Latempa, C. A. Grimes, *Sens. Lett.* **2006**, *4*, 334.
[84] C. A. Grimes, *J. Mater. Chem.* **2007**, *17*, 1451.
[85] G. K. Mor, O. K. Varghese, M. Paulose, K. Shankar, C. A. Grimes, *Sol. Energy Mater. Sol. Cells* **2006**, *90*, 2011.
[86] J. S. Beck, J. C. Vartuli, W. J. Roth, M. E. Leonowicz, C. T. Kresge, K. D. Schmitt, C. T. W. Chu, D. H. Olson, E. W. Sheppard, S. B. McCullen, J. B. Higgins, J. L. Schlenker, *J. Am. Chem. Soc.* **1992**, *114*, 10834.
[87] C. T. Kresge, M. E. Leonowicz, W. J. Roth, J. C. Vartuli, J. S. Beck, *Nature* **1992**, *359*, 710.

[88] S. Inagaki, Y. Fukushima, K. Kuroda, *J. Chem. Soc. Chem. Commun.* **1993**, 680.
[89] M. Trau, N. Yao, E. Kim, Y. Xia, G. M. Whitesides, I. A. Aksay, *Nature* **1997**, *390*, 674.
[90] T. L. Morkved, M. Lu, A. M. Urbas, E. E. Ehrichs, H. M. Jaeger, P. Mansky, T. P. Russell, *Science* **1996**, *273*, 931.
[91] D. Wang, X. Ji, J.-B. Pang, Q. Hu, H. Xu, Y. Lu, *Phys. Chem. Chem. Phys.* **2003**, *5*, 4070.
[92] A. Firouzi, D. J. Schaefer, S. H. Tolbert, G. D. Stucky, B. F. Chmelka, *J. Am. Chem. Soc.* **1997**, *119*, 9466.
[93] S. H. Tolbert, A. Firouzi, G. D. Stucky, B. F. Chmelka, *Science* **1997**, *278*, 264.
[94] N. A. Melosh, P. Davidson, P. Feng, D. J. Pine, B. F. Chmelka, *J. Am. Chem. Soc.* **2001**, *123*, 1240.
[95] D. H. Wang, R. Kou, Z. L. Yang, J. B. He, Z. Z. Yang, Y. F. Lu, *Chem. Commun.* **2005**, 166.
[96] G. Kim, M. Libera, *Macromolecules* **1998**, *31*, 2569.
[97] A. L. Briseno, J. Aizenberg, Y. J. Han, R. A. Penkala, H. Moon, A. J. Lovinger, C. Kloc, Z. A. Bao, *J. Am. Chem. Soc.* **2005**, *127*, 12164.
[98] S. Yang, C. K. Ullal, E. L. Thomas, G. Chen, J. Aizenberg, *Appl. Phys. Lett.* **2005**, *86*, 201121.
[99] J. Aizenberg, *Adv. Mater.* **2004**, *16*, 1295.
[100] D. M. Chapin, C. S. Fuller, G. L. Pearson, *J. Appl. Phys.* **1954**, *25*, 676.
[101] W. Shockley, H. J. Queisser, *J. Appl. Phys.* **1961**, *32*, 510.
[102] N. G. Dherea, R. G. Dhere, *J. Vac. Sci. Technol., A* **2005**, *23*, 1208.
[103] C. R. Wronski, D. E. Carlson, R. E. Daniel, *Appl. Phys. Lett.* **1976**, *29*, 602.
[104] D. E. Carlson, C. R. Wronski, *Appl. Phys. Lett.* **1976**, *28*, 671.
[105] D. E. Carlson, J. I. Pankove, C. R. Wronski, P. J. Zanzucchi, *Thin Solid Films* **1977**, *45*, 43.
[106] D. E. Carlson, C. R. Wronski, *J. Electron. Mater.* **1977**, *6*, 95.
[107] D. E. Carlson, C. R. Wronski, J. I. Pankove, P. J. Zanzucchi, D. L. Staebler, *RCA Rev.* **1977**, *38*, 211.
[108] S. R. Ovshinsky, *J. Vac. Sci. Technol., B* **1984**, *2*, 835.
[109] S. R. Ovshinsky, A. Madan, *Nature* **1978**, *276*, 482.
[110] C. R. Wronski, *IEEE Trans. Electron Devices* **1977**, *24*, 351.
[111] P. J. Zanzucchi, C. R. Wronski, D. E. Carlson, *J. Appl. Phys.* **1977**, *48*, 5227.
[112] T. L. Chu, *J. Electrochem. Soc.* **1977**, *124*, C303.
[113] T. L. Chu, *J. Cryst. Growth* **1977**, *39*, 45.
[114] T. L. Chu, S. S. Chu, K. Y. Duh, H. I. Yoo, *IEEE Trans. Electron Devices* **1977**, *24*, 442.
[115] T. L. Chu, G. A. Vanderleeden, S. C. Chu, J. R. Boyd, *J. Electrochem. Soc.* **1977**, *124*, C105.
[116] A. Bosio, N. Romeo, S. Mazzamuto, V. Canevari, *Prog. Cryst. Growth Character. Mater.* **2006**, *52*, 247.
[117] G. Khrypunov, A. Romeo, F. Kurdesau, D. L. Batzner, H. Zogg, A. N. Tiwari, *Sol. Energy Mater. Sol. Cells* **2006**, *90*, 664.
[118] X. Z. Wu, *Solar Energy* **2004**, *77*, 803.
[119] C. S. Ferekides, U. Balasubramanian, R. Mamazza, V. Viswanathan, H. Zhao, D. L. Morel, *Solar Energy* **2004**, *77*, 823.
[120] X. Mathew, J. P. Enriquez, A. Romeo, A. N. Tiwari, *Solar Energy* **2004**, *77*, 831.
[121] K. Zweibel, J. Mason, V. Fthenakis, *Sci. Am.* **2008**, *298*, 64.
[122] S. Wagner, J. L. Shay, P. Migliora, H. M. Kasper, *Appl. Phys. Lett.* **1974**, *25*, 434.
[123] M. Altosaar, M. Danilson, M. Kauk, J. Krustok, E. Mellikov, J. Raudoja, K. Timmo, T. Varema, *Sol. Energy Mater. Sol. Cells* **2005**, *87*, 25.
[124] K. W. Mitchell, W. Chesarek, D. R. Willett, C. Eberspacher, J. H. Ermer, R. R. Gay, *Solar Cells* **1991**, *30*, 131.
[125] N. G. Dhere, *Sol. Energy Mater. Sol. Cells* **2007**, *91*, 1376.
[126] M. Bar, N. Allsop, I. Lauermann, C. H. Fischer, *Appl. Phys. Lett.* **2007**, *90*, 132 118.
[127] J. Palm, V. Probst, F. H. Karg, *Solar Energy* **2004**, *77*, 757.
[128] K. P. Jayadevan, T. Y. Tseng, *J. Nanosci. Nanotechnol.* **2005**, *5*, 1768.
[129] K. Q. Peng, Y. Xu, Y. Wu, Y. J. Yan, S. T. Lee, J. Zhu, *Small* **2005**, *1*, 1062.
[130] M. Grätzel, *Nature* **2000**, *403*, 363.
[131] M. Grätzel, *Actualite Chimique* **2007**, 57.
[132] J. M. Kroon, N. J. Bakker, H. J. P. Smit, P. Liska, K. R. Thampi, P. Wang, S. M. Zakeeruddin, M. Grätzel, A. Hinsch, S. Hore, U. Wurfel, R. Sastrawan, J. R. Durrant, E. Palomares, H. Pettersson, T. Gruszecki, J. Walter, K. Skupien, G. E. Tulloch, *Prog. Photovoltaics* **2007**, *15*, 1.
[133] P. Liska, K. R. Thampi, M. Grätzel, D. Bremaud, D. Rudmann, H. M. Upadhyaya, A. N. Tiwari, *Appl. Phys. Lett.* **2006**, *88*, 203103.
[134] M. Law, L. E. Greene, J. C. Johnson, R. Saykally, P. D. Yang, *Nat. Mater.* **2005**, *4*, 455.
[135] S. Kim, J. K. Lee, S. O. Kang, J. Ko, J. H. Yum, S. Fantacci, F. De Angelis, D. Di Censo, M. K. Nazeeruddin, M. Grätzel, *J. Am. Chem. Soc.* **2006**, *128*, 16701.
[136] B. Li, L. D. Wang, B. N. Kang, P. Wang, Y. Qiu, *Sol. Energy Mater. Sol. Cells* **2006**, *90*, 549.
[137] B. Pradhan, S. K. Batabyal, A. J. Pal, *Sol. Energy Mater. Sol. Cells* **2007**, *91*, 769.
[138] J. B. Baxter, A. M. Walker, K. van Ommering, E. S. Aydil, *Nanotechnology* **2006**, *17*, S304.
[139] M. Law, L. E. Greene, A. Radenovic, T. Kuykendall, J. Liphardt, P. D. Yang, *J. Phys. Chem. B* **2006**, *110*, 22652.
[140] K. Zhu, N. R. Neale, A. Miedaner, A. J. Frank, *Nano Lett.* **2007**, *7*, 69.
[141] W. L. Wang, H. Lin, J. B. Li, N. Wang, *J. Am. Ceram. Soc.* **2008**, *91*, 628.
[142] T. P. Chou, Q. F. Zhang, G. E. Fryxell, G. Z. Cao, *Adv. Mater.* **2007**, *19*, 2588.
[143] Q. F. Zhang, T. P. Chou, B. Russo, S. A. Jenekhe, G. Z. Cao, *Angew. Chem.* **2008**, *120*, 2436; *Angew. Chem. Int. Ed.* **2008**, *47*, 2402.
[144] Q. F. Zhang, T. P. Chou, B. Russo, S. A. Jenekhe, G. Z. Cao, *Adv. Funct. Mater.* **2008**, *18*, 1654.
[145] D. Jezequel, J. Guenot, N. Jouini, F. Fievet, *J. Mater. Res.* **1995**, *10*, 77.
[146] R. J. Ellingson, J. B. Asbury, S. Ferrere, H. N. Ghosh, J. R. Sprague, T. Q. Lian, A. J. Nozik, *J. Phys. Chem. B* **1998**, *102*, 6455.
[147] M. K. Nazeeruddin, A. Kay, I. Rodicio, R. Humphry-Baker, E. Muller, P. Liska, N. Vlachopoulos, M. Grätzel, *J. Am. Chem. Soc.* **1993**, *115*, 6382.
[148] K. Keis, C. Bauer, G. Boschloo, A. Hagfeldt, K. Westermark, H. Rensmo, H. Siegbahn, *J. Photochem. Photobiol. A* **2002**, *148*, 57.
[149] J. E. Rannels, *Sol. Energy Mater. Sol. Cells* **2001**, *65*, 3.
[150] M. Yamaguchi, T. Takamoto, A. Khan, M. Imaizumi, S. Matsuda, N. J. Ekins-Daukes, *Prog. Photovoltaics* **2005**, *13*, 125.
[151] A. Shabaev, A. L. Efros, A. J. Nozik, *Nano Lett.* **2006**, *6*, 2856.
[152] V. I. Klimov, *J. Phys. Chem. B* **2006**, *110*, 16827.
[153] R. D. Schaller, J. M. Pietryga, V. I. Klimov, *Nano Lett.* **2007**, *7*, 3469.
[154] J. E. Murphy, M. C. Beard, A. G. Norman, S. P. Ahrenkiel, J. C. Johnson, P. R. Yu, O. I. Micic, R. J. Ellingson, A. J. Nozik, *J. Am. Chem. Soc.* **2006**, *128*, 3241.
[155] R. D. Schaller, M. A. Petruska, V. I. Klimov, *Appl. Phys. Lett.* **2005**, *87*, 253102.
[156] M. C. Beard, K. P. Knutsen, P. R. Yu, J. M. Luther, Q. Song, W. K. Metzger, R. J. Ellingson, A. J. Nozik, *Nano Lett.* **2007**, *7*, 2506.
[157] R. J. Ellingson, M. C. Beard, J. C. Johnson, P. R. Yu, O. I. Micic, A. J. Nozik, A. Shabaev, A. L. Efros, *Nano Lett.* **2005**, *5*, 865.
[158] R. D. Schaller, M. Sykora, J. M. Pietryga, V. I. Klimov, *Nano Lett.* **2006**, *6*, 424.
[159] F. Schedin, A. K. Geim, S. V. Morozov, E. W. Hill, P. Blake, M. I. Katsnelson, K. S. Novoselov, *Nat. Mater.* **2007**, *6*, 652.
[160] US DOE Office of Basic Energy Sciences, *Energy Needs for Electrical Energy Storage: Report of the Basic Energy Science Workshop on Electrical Energy Storage*, **2007**.
[161] A. Burke, *J. Power Sources* **2000**, *91*, 37.
[162] R. Kotz, M. Carlen, *Electrochim. Acta* **2000**, *45*, 2483.
[163] M. Anderman, *Briefing to the US Senate Committee in Energy and Natural Resources*, **2007**.
[164] US Department of Energy, Energy Efficiency and Renewable Energy (EERE), *Annual Progress Report: Energy Storage Development*, **2005**.
[165] US Department of Energy, Energy Efficiency and Renewable Energy (EERE), *Energy Storage Research and Development Annual Progress Report*, **2006**; http://www1.eere.energy.gov/vehiclesandfuels/pdfs/program/2006_energy_storage.pdf.
[166] US Department of Energy, Energy Efficiency and Renewable Energy (EERE), *Summary Report—Discussion Meeting on Plug-In Hybrid Electricle Vehicles*, **2006**; http://www1.eere.energy.gov/vehiclesandfuels/pdfs/program/plug-in_summary_rpt.pdf.
[167] US DOE Office of Basic Energy Sciences, *Report of the Basic Energy Sciences Workshop on Electrochemical Energy Storage*, **2007**; http://www.science.doe.gov/bes/reports/files/EES_rpt.pdf
[168] J. M. Tarascon, M. Armand, *Nature* **2001**, *414*, 359.
[169] M. K. Datta, P. N. Kumta, *J. Power Sources* **2006**, *158*, 557.

[170] US DOE, Sandia National Laboratory, News Release **2003**: http://www.sandia.gov/news-center/news-release/2003/renew-energy-batt/betterlithium.html.
[171] M. N. Obrovac, L. Christensen, *Electrochem. Solid-State Lett.* **2004**, *7*, A93.
[172] T. D. Hatchard, J. R. Dahn, *J. Electrochem. Soc.* **2004**, *151*, A838.
[173] I. Yonezu, S. Yoshimura, S. Fujitani, T. Nohma, *Abstract 58, IMLB 2006: 12th International Meeting on Lithium Batteries* (Biarritz, France), June 18–23, **2006**.
[174] C. K. Chan, H. Peng, G. Liu, K. Mcliwrath, X. F. Zhang, R. A. Huggins, Y. Cui, *Nat. Nanotechnol.* **2007**, *3*, 31.
[175] C. K. Chan, X. F. Zhang, Y. Cui, *Nano Lett.* **2008**, *8*, 307.
[176] T. Ohzuku, Z. Takehara, S. Yoshizawa, *Electrochim. Acta* **1979**, *24*, 219.
[177] L. Kavan, D. Fattakhova, P. Krtil, *J. Electrochem. Soc.* **1999**, *146*, 1375.
[178] M. V. Koudriachova, N. M. Harrison, S. W. de Leeuw, *Phys. Rev. Lett.* **2001**, *86*, 1275.
[179] M. V. Koudriachova, S. W. de Leeuw, N. M. Harrison, *Chem. Phys. Lett.* **2003**, *371*, 150.
[180] E. Baudrin, S. Cassaignon, M. Koesch, J. P. Jolivet, L. Dupont, J. M. Tarascon, *Electrochem. Commun.* **2007**, *9*, 337.
[181] Y. S. Hu, L. Kienle, Y. G. Guo, J. Maier, *Adv. Mater.* **2006**, *18*, 1421.
[182] M. A. Reddy, M. S. Kishore, V. Pralong, V. Caignaert, U. V. Varadaraju, B. Raveau, *Electrochem. Commun.* **2006**, *8*, 1299.
[183] C. H. Jiang, I. Honma, T. Kudo, H. S. Zhou, *Electrochem. Solid-State Lett.* **2007**, *10*, A127.
[184] G. Sudant, E. Baudrin, D. Larcher, J.-M. Tarascon, *J. Mater. Chem.* **2005**, *15*, 1263.
[185] D. H. Wang, D. Choi, G. Z. Yang, V. V. Viswanathan, Z. Nie, C. M. Wang, Y. J. Song, J. G. Zhang, J. Liu, *Chem. Mater.* **2008**, *20*, 3435.
[186] K. Lee, Y. Wang, G. Z. Cao, *J. Phys. Chem. B* **2005**, *109*, 16700.
[187] D. W. C. Liu, Q. F. Zhang, P. Xiao, B. B. Garcia, Q. Guo, R. Champion, G. Z. Cao, *Chem. Mater.* **2008**, *20*, 1376.
[188] K. Takahashi, Y. Wang, K. Lee, G. Z. Cao, *Appl. Phys. A: Mater. Sci. Process.* **2006**, *82*, 27.
[189] J. Kim, J. Cho, *J. Electrochem. Soc.* **2007**, *154*, A542.
[190] J. Kim, J. Cho, *Electrochem. Solid-State Lett.* **2007**, *10*, A81.
[191] J. W. Xu, C. H. Ha, B. Cao, W. F. Zhang, *Electrochim. Acta* **2007**, *52*, 8044.
[192] Q. Wang, Z. H. Wen, J. H. Li, *Inorg. Chem.* **2006**, *45*, 6944.
[193] A. R. Armstrong, G. Armstrong, J. Canales, P. G. Bruce, *J. Power Sources* **2005**, *146*, 501.
[194] G. Armstrong, A. R. Armstrong, J. Canales, P. G. Bruce, *Electrochem. Solid-State Lett.* **2006**, *9*, A139.
[195] A. R. Armstrong, G. Armstrong, J. Canales, R. Garcia, P. G. Bruce, *Adv. Mater.* **2005**, *17*, 862.
[196] K. Takahashi, S. J. Limmer, Y. Wang, G. Z. Cao, *J. Phys. Chem. B* **2004**, *108*, 9795.
[197] Y. Wang, K. Takahashi, H. M. Shang, G. Z. Cao, *J. Phys. Chem. B* **2005**, *109*, 3085.
[198] K. Takahashi, Y. Wang, G. Z. Cao, *Appl. Phys. Lett.* **2005**, *86*, 053102.
[199] Y. Wang, G. Z. Cao, *J. Mater. Chem.* **2007**, *17*, 894.
[200] P. Xiao, B. B. Garcia, Q. Guo, D. W. Liu, G. Z. Cao, *Electrochem. Commun.* **2007**, *9*, 2441.
[201] K. Takahashi, Y. Wang, G. Z. Cao, *J. Phys. Chem. B* **2005**, *109*, 48.
[202] S. J. Limmer, G. Z. Cao, *Adv. Mater.* **2003**, *15*, 427.
[203] S. J. Limmer, T. P. Chou, G. Z. Cao, *J. Mater. Sci.* **2004**, *39*, 895.
[204] S. J. Limmer, T. P. Chou, G. Z. Cao, *J. Sol-Gel Sci. Technol.* **2005**, *36*, 183.
[205] S. J. Limmer, S. V. Cruz, G. Z. Cao, *Appl. Phys. A: Mater. Sci. Process.* **2004**, *79*, 421.
[206] S. J. Limmer, T. L. Hubler, G. Z. Cao, *J. Sol-Gel Sci. Technol.* **2003**, *26*, 577.
[207] S. J. Limmer, S. Seraji, M. J. Forbess, Y. Wu, T. P. Chou, C. Nguyen, G. Z. Cao, *Adv. Mater.* **2001**, *13*, 1269.
[208] S. J. Limmer, S. Seraji, Y. Wu, T. P. Chou, C. Nguyen, G. Z. Cao, *Adv. Funct. Mater.* **2002**, *12*, 59.
[209] G. Z. Cao, *J. Phys. Chem. B* **2004**, *108*, 19921.
[210] Y. Wang, G. Z. Cao, *Electrochim. Acta* **2006**, *51*, 4865.
[211] Y. Wang, K. Takahashi, K. Lee, G. Z. Cao, *Adv. Funct. Mater.* **2006**, *16*, 1133.
[212] Y. Wang, G. Z. Cao, *Chem. Mater.* **2006**, *18*, 2787.
[213] T. Maxisch, F. Zhou, G. Ceder, *Phys. Rev. B* **2006**, *73*, 104301.
[214] A. Yamada, H. Koizumi, S. I. Nishimura, N. Sonoyama, R. Kanno, M. Yonemura, T. Nakamura, Y. Kobayashi, *Nat. Mater.* **2006**, *5*, 357.
[215] C. Delacourt, P. Poizot, J. M. Tarascon, C. Masquelier, *Nat. Mater.* **2005**, *4*, 254.
[216] C. Delacourt, P. Poizot, S. Levasseur, C. Masquelier, *Electrochem. Solid-State Lett.* **2006**, *9*, A352.
[217] N. Meethong, H. Y. S. Huang, W. C. Carter, Y. M. Chiang, *Electrochem. Solid-State Lett.* **2007**, *10*, A134.
[218] D. Choi, P. N. Kumta, *J. Power Sources* **2007**, *163*, 1064.
[219] P. Poizot, S. Laruelle, S. Grugeon, L. Dupont, J. M. Tarascon, *Nature* **2000**, *407*, 496.
[220] L. Taberna, S. Mitra, P. Poizot, P. Simon, J. M. Tarascon, *Nat. Mater.* **2006**, *5*, 567.
[221] J. M. Tarascon, A. S. Gozdz, C. Schmutz, F. Shokoohi, P. C. Warren, *Solid State Ionics* **1996**, *86–88*, 49.
[222] S. Mitra, P. Poizot, A. Finke, J. M. Tarascon, *Adv. Funct. Mater.* **2006**, *16*, 2281.
[223] M. Doyle, J. Newman, J. Reimers, *J. Power Sources* **1994**, *52*, 211.
[224] E. Frackowiak, *Phys. Chem. Chem. Phys.* **2007**, *9*, 1774.
[225] B. E. Conway, *J. Electrochem. Soc.* **1991**, *138*, 1539.
[226] F. Pico, J. M. Rojo, M. L. Sanjuan, A. Anson, A. M. Benito, M. A. Callejas, W. K. Maser, M. T. Martinez, *J. Electrochem. Soc.* **2004**, *151*, A831.
[227] E. Frackowiak, K. Metenier, V. Bertagna, F. Beguin, *Appl. Phys. Lett.* **2000**, *77*, 2421.
[228] J. P. Zheng, T. R. Jow, *J. Power Sources* **1996**, *62*, 155.
[229] J. P. Zheng, T. R. Jow, *J. Electrochem. Soc.* **1995**, *142*, L6.
[230] R. Q. Fu, Z. R. Ma, J. P. Zheng, *J. Phys. Chem. B* **2002**, *106*, 3592.
[231] Z. R. Ma, J. P. Zheng, R. Q. Fu, *Chem. Phys. Lett.* **2000**, *331*, 64.
[232] Z. A. Zhang, B. C. Yang, M. G. Deng, Y. D. Hu, *Int. J. Inorg. Mater.* **2005**, *20*, 529.
[233] D. Choi, P. N. Kumta, *J. Electrochem. Soc.* **2006**, *153*, A2298.
[234] D. Choi, P. N. Kumta, *Electrochem. Solid-State Lett.* **2005**, *8*, A418.
[235] T. C. Liu, W. G. Pell, B. E. Conway, S. L. Roberson, *J. Electrochem. Soc.* **1998**, *145*, 1882.
[236] D. Choi, G. E. Blomgren, P. N. Kumta, *Adv. Mater.* **2006**, *18*, 1178.
[237] J. H. Chen, W. Z. Li, D. Z. Wang, S. X. Yang, J. G. Wen, Z. F. Ren, *Carbon* **2002**, *40*, 1193.
[238] J. N. Barisci, G. G. Wallace, R. H. Baughman, *J. Electroanal. Chem.* **2000**, *488*, 92.
[239] M. W. Xu, D. D. Zhao, S. J. Bao, H. L. Li, *J. Solid State Electrochem.* **2007**, *11*, 1101.
[240] S. Yamazaki, K. Obata, Y. Okuhama, Y. Matsuda, M. Ishikawa, *Electrochemistry* **2007**, *75*, 592.
[241] A. L. M. Reddy, S. Ramaprabhu, *J. Phys. Chem. C* **2007**, *111*, 7727.
[242] K. Jurewicz, S. Delpeux, V. Bertagna, F. Beguin, E. Frackowiak, *Chem. Phys. Lett.* **2001**, *347*, 36.
[243] E. Raymundo-Pinero, V. Khomenko, E. Frackowiak, F. Beguin, *J. Electrochem. Soc.* **2005**, *152*, A229.
[244] E. Frackowiak, V. Khomenko, K. Jurewicz, K. Lota, F. Beguin, *J. Power Sources* **2006**, *153*, 413.
[245] V. Khomenko, E. Raymundo-Pinero, F. Beguin, *J. Power Sources* **2006**, *153*, 183.
[246] J. Chmiola, G. Yushin, Y. Gogotsi, C. Portet, P. Simon, P. L. Taberna, *Science* **2006**, *313*, 1760.
[247] D. N. Futaba, K. Hata, T. Yamada, T. Hiraoka, Y. Hayamizu, Y. Kakudate, O. Tanaike, H. Hatori, M. Yumura, S. Iijima, *Nat. Mater.* **2006**, *5*, 987.
[248] Y. G. Wang, H. Q. Li, Y. Y. Xia, *Adv. Mater.* **2006**, *18*, 2619.
[249] X. H. Zhou, S. Zhang, M. H. Shi, J. L. Kong, *J. Solid State Electrochem.* **2007**, *11*, 317.
[250] V. Gupta, N. Miura, *Electrochem. Solid-State Lett.* **2005**, *8*, A630.
[251] Q. F. Wu, K. X. He, H. Y. Mi, X. G. Zhang, *Mater. Chem. Phys.* **2007**, *101*, 367.
[252] X. Y. Wang, X. Y. Wang, W. G. Huang, P. J. Sebastian, S. Gamboa, *J. Power Sources* **2005**, *140*, 211.
[253] X. Y. Chen, X. X. Li, Y. Jiang, C. W. Shi, X. L. Li, *Solid State Commun.* **2005**, *136*, 94.
[254] M. S. Wu, *Appl. Phys. Lett.* **2005**, *87*, 153102.
[255] P. Ragupathy, H. N. Vasan, N. Munichandraiah, *J. Electrochem. Soc.* **2008**, *155*, A34.
[256] M. Subhramannia, B. K. Balan, B. R. Sathe, I. S. Mulla, V. K. Pillai, *J. Phys. Chem. C* **2007**, *111*, 16593.
[257] G. Y. Zhao, C. L. Xu, H. L. Li, *J. Power Sources* **2007**, *163*, 1132.
[258] V. Gupta, N. Miura, *Mater. Lett.* **2006**, *60*, 1466.

[259] C. L. Xu, S. J. Bao, L. B. Kong, H. Li, H. L. Li, *J. Solid State Chem.* **2006**, *179*, 1351.
[260] Y. T. Wu, C. C. Hu, *Electrochem. Solid-State Lett.* **2005**, *8*, A240.
[261] D. K. C. MacDonald, *Thermoelectricity: An Introduction to the Principles*, Wiley, New York, **1962**.
[262] K. A. Chao, M. Larsson, *Solid State Commun.* **2006**, *139*, 490.
[263] Y. M. Lin, X. Z. Sun, M. S. Dresselhaus, *Phys. Rev. B* **2000**, *62*, 4610.
[264] A. L. Prieto, M. S. Sander, M. Martin-Gonzalez, R. Gronsky, T. Sands, A. M. Stacy, *J. Am. Chem. Soc.* **2001**, *123*, 7160.
[265] D. S. Xu, Y. J. Xu, D. P. Chen, G. L. Guo, L. L. Gui, Y. Q. Tang, *Adv. Mater.* **2000**, *12*, 520.
[266] C. G. Jin, G. Q. Zhang, T. Qian, X. G. Li, Z. Yao, *J. Phys. Chem. B* **2005**, *109*, 1430.
[267] W. Wang, F. L. Jia, Q. H. Huang, J. Z. Zhang, *Microelectron. Eng.* **2005**, *77*, 223.
[268] S. B. Cronin, Y. M. Lin, T. Koga, X. Sun, J. Y. Ying, M. S. Dresselhaus, *IEEE—18th International Conference on Thermoelectrics (1999): ICT Symposium Proceedings* (Ed.: G. Chen), IEEE, Piscataway, NJ, **2000**, 554.
[269] J. R. Lim, J. F. Whitacre, J. P. Fleurial, C. K. Huang, M. A. Ryan, N. V. Myung, *Adv. Mater.* **2005**, *17*, 1488.
[270] A. I. Hochbaum, R. K. Chen, R. D. Delgado, W. J. Liang, E. C. Garnett, M. Najarian, A. Majumdar, P. D. Yang, *Nature* **2008**, *451*, 163.
[271] M. S. Dresselhaus, G. Chen, M. Y. Tang, R. G. Yang, H. Lee, D. Z. Wang, Z. F. Ren, J. P. Fleurial, P. Gogna, *Adv. Mater.* **2007**, *19*, 1043.
[272] A. I. Boukai, Y. Bunimovich, J. Tahir-Kheli, J. K. Yu, W. A. Goddard, J. R. Heath, *Nature* **2008**, *451*, 168.
[273] A. Boukai, K. Xu, J. R. Heath, *Adv. Mater.* **2006**, *18*, 864.
[274] US DOE Office of Science, *Directing Matter and Energy: Five Challenges for Science and Imagination*, **2005**.
[275] K. D. Kreuer, *Chem. Mater.* **1996**, *8*, 610.
[276] K. D. Kreuer, S. J. Paddison, E. Spohr, M. Schuster, *Chem. Rev.* **2004**, *104*, 4637.
[277] B. Smitha, S. Sridhar, A. A. Khan, *J. Membr. Sci.* **2005**, *259*, 10.
[278] W. H. J. Hogarth, J. C. D. da Costa, G. Q. Lu, *J. Power Sources* **2005**, *142*, 223.
[279] K. Schmidt-Rohr, Q. Chen, *Nat. Mater.* **2008**, *7*, 75.
[280] *Information for the Public from The Royal Swedish Academy of Sciences*: http://nobelprize.org/nobel_prizes/chemistry/laureates/2003/public.html.
[281] M. Akeson, D. W. Deamer, *Biophys. J.* **1991**, *60*, 101.
[282] R. Pomes, B. Roux, *Biophys. J.* **1996**, *71*, 19.
[283] R. Pomes, B. Roux, *Biophys. J.* **1996**, *70*, A263.
[284] R. Pomes, B. Roux, *Biophys. J.* **1996**, *70*, TUPM4.
[285] G. M. Preston, T. P. Carroll, W. B. Guggino, P. Agre, *Science* **1992**, *256*, 385.
[286] D. A. Doyle, J. M. Cabral, R. A. Pfuetzner, A. L. Kuo, J. M. Gulbis, S. L. Cohen, B. T. Chait, R. MacKinnon, *Science* **1998**, *280*, 69.
[287] R. Pomes, B. Roux, *Biophys. Chem.* **1998**, *75*, 33.
[288] G. Hummer, *Mol. Phys.* **2007**, *105*, 201.
[289] D. Nepal, K. E. Geckeler, *Small* **2007**, *3*, 1259.
[290] D. Y. Zhao, J. L. Feng, Q. S. Huo, N. Melosh, G. H. Fredrickson, B. F. Chmelka, G. D. Stucky, *Science* **1998**, *279*, 548.
[291] X. Feng, G. E. Fryxell, L. Q. Wang, A. Y. Kim, J. Liu, K. M. Kemner, *Science* **1997**, *276*, 923.
[292] Y. S. Shin, J. Liu, L. Q. Wang, Z. M. Nie, W. D. Samuels, G. E. Fryxell, G. J. Exarhos, *Angew. Chem.* **2000**, *112*, 2814; *Angew. Chem. Int. Ed.* **2000**, *39*, 2702.
[293] M. W. W. Adams, *Biochim. Biophys. Acta* **1990**, *1020*, 115.
[294] A. E. Przybyla, J. Robbins, N. Menon, H. D. Peck, *FEMS Microbiol. Rev.* **1992**, *88*, 109.
[295] Z. L. Wang, J. H. Song, *Science* **2006**, *312*, 242.
[296] X. D. Wang, J. H. Song, J. Liu, Z. L. Wang, *Science* **2007**, *316*, 102.
[297] Y. Qin, X. D. Wang, Z. L. Wang, *Nature* **2008**, *451*, 809.
[298] B. Z. Tian, X. L. Zheng, T. J. Kempa, Y. Fang, N. F. Yu, G. H. Yu, J. L. Huang, C. M. Lieber, *Nature* **2007**, *449*, 885.
[299] Y. Wang, G. Z. Cao, *Adv. Mater.* **2008**, *20*, 2251.
[300] R. W. Pekala, *J. Mater. Sci.* **1989**, *24*, 3221.
[301] A. Feaver, G. Z. Cao, *Carbon* **2006**, *44*, 590.
[302] A. Burke, *J. Power Sources* **2000**, *91*, 37.
[303] B. B. Garcia, A. Feaver, G. F. Zhang, R. Champion, G. Z. Cao, T. T. Fisher, K. P. Nagle, G. T. Seidler, *J. Appl. Phys.* **2008**, *104*, 014305.

Received: April 21, 2008
Published online on August 11, 2008

